ENHANCING PULMONARY DRUG DISPERSION USING LIPID SURFACTANTS IN A MURINE MODEL

by

Morgan Midgett

B.A. in Biological Sciences, Carnegie Mellon University, 2013

Submitted to the Graduate Faculty of

the Department of Infectious Diseases and Microbiology

Graduate School of Public Health in partial fulfillment

of the requirements for the degree of

Master of Science

University of Pittsburgh

2017

UNIVERSITY OF PITTSBURGH

GRADUATE SCHOOL OF PUBLIC HEALTH

This thesis was presented

by

Morgan Midgett

It was defended on

April 6th 2017

and approved by

Amy L. Hartman, PhD, Assistant Professor, Department of Infectious Diseases and Microbiology, Graduate School of Public Health, University of Pittsburgh

Simon M. Barratt-Boyes, BVSc, PhD, Professor, Department of Infectious Diseases and Microbiology, Graduate School of Public Health, University of Pittsburgh

Thesis director: Douglas S. Reed, PhD, Associate Professor, Department of Immunology, School of Medicine, University of Pittsburgh

Douglas S. Reed, PhD

ENHANCING PULMONARY DRUG DISPERSION USING LIPID SURFACTANTS IN A MURINE MODEL

Morgan Midgett, MS

University of Pittsburgh, 2017

ABSTRACT

Cystic fibrosis is a life-shortening genetic disease that affects the respiratory, digestive and reproductive systems. Though it manifests a variety of symptoms, it is most notably characterized by chronic pulmonary infections that ultimately lead to respiratory failure and premature death. Recent research has focused on developing inhaled aerosol antibiotics to treat such infections; however, current formulations use saline liquid carriers that are unable to fully disperse the drugs throughout the lungs, as the surface tension of saline is much higher than the surface tension of the airway liquid surface. Given that certain lipid surfactants are capable of lowering the surface tension of aqueous solutions, our hypothesis is that a surfactant-based liquid carrier could greatly improve pulmonary drug dispersion and efficacy to better treat lung infections. Previous work both *in vitro* and in a small group of cystic fibrosis patients has led to the creation of an optimized, self-dispersing inhaled carrier formation that significantly enhances aerosolized drug spreading under very specific, laboratory conditions. The aims of this project are to develop an *in vivo* imaging model to assess pulmonary drug dispersion, and then to use this model to determine if our surfactant-based formulation also improves drug dispersion in a murine model. To model drug dispersal in the lungs, we instilled BL/6 mice with a combination of fluorescent dye and either water or surfactant, and then measured the amount of fluorescence in different planar regions of the lungs. We then calculated the ratio of fluorescence in the peripheral lung regions to the total

fluorescence in the lungs, and used this to compare the mice instilled with water/dye solution to those instilled with surfactant/dye solution ($p = 0.0287$). ***Public health significance:*** Our results suggest that our candidate surfactant significantly increases pulmonary drug dispersion in the murine airways, and future studies are necessary to confirm these findings in human subjects. We hope that future research can build upon our early results to create an optimal inhaled antibiotic capable of fully eradicating CF-related pulmonary infections and improving patient outcomes.

TABLE OF CONTENTS

LIST OF TABLES

LIST OF FIGURES

ACKNOWLEDGEMENT

First and foremost, I want to thank my mentor and thesis director, Dr. Douglas Reed, for guiding and supporting me over the last two years. This project has been full unexpected surprises that were both frustrating and disappointing at times, but Dr. Reed's unrelenting encouragement carried me through until the very end. I am also very grateful to him for understanding my financial need to work part-time throughout this program, and for making accommodations for my hectic schedule – few PI's would have done the same. I also extend this thank you to Katherine Willet, who very patiently trained me in most of the laboratory procedures. A special thanks to you, Katie, for serving as a friend as well as a mentor, and for providing life-guidance in addition to lab-guidance.

To Dr. Amy Hartman and Dr. Simon Barratt-Boyes, thank you for your time and support, as well as for all of your helpful criticisms. I chose you both because I so highly respect you -- both in the classroom and in the lab -- and it means a great deal to me that you both took the time out of your hectic schedules to serve on my committee.

Though he may never see this, I also want to thank my inspiration for entering this program – Dr. Jim Williams of Carnegie Mellon University. You were among my favorite undergraduate professors, and are the only reason I ever picked up a virology textbook. I still remember fondly the afternoons I spent in your office listening to stories of your past, and I hope one day I can thank you in person for leading me down this path.

Finally, in the most sentimental of acknowledgements, I want to thank the man who supported me at home during this entire journey, and who never stopped loving me no matter how crazy and stressed out I got: Jesse Kiefer. Not only did you give me the push I needed to go back

to school, but you were the rock that kept me together during the times I wanted to give up. Thank you, from the bottom of my heart.

1.0 INTRODUCTION

Cystic fibrosis (CF) is an incurable genetic disease that affects the respiratory, digestive and reproductive systems. Although CF manifests a variety of symptoms, it is most notably characterized by chronic pulmonary infections that ultimately lead to respiratory failure and premature death. CF is caused by a defect in the cystic fibrosis transmembrane conductance regulator (CFTR) gene, which encodes an ion channel protein responsible for regulating chloride and thiocyanate transport across lung epithelial cells (1). To date, over 1,900 disease-causing mutations have been characterized in the CFTR protein, resulting in a wide-spectrum of disease severity (2). However, one mutation -- ΔF508 –accounts for about 70% of CF cases, and results in the premature degradation of the CFRT protein (3).

Though the CFTR protein is also found in the liver, pancreas, skin, and reproductive and digestive tracts, the most serious complications of CF arise from the malfunctioning of CFTR in the lungs. When CFTR is functioning properly, negatively charged chloride and thiocyanate ions are actively transported out of lung epithelial cells into the surrounding airway surface liquid (ASL) – the thin layer of fluid that exists between the airway epithelial cell apical surface and the mucus layer. It also acts to regulate the epithelial sodium channel protein, ENac, through an unknown mechanism to prevent sodium and water flow out of the ASL and into the cell epithelium. When CFTR is malfunctioning, however, ion movement out of the cell is blocked, and ion movement into the cell by ENac is unregulated (4). There are several theories regarding how these

changes result in the clinical manifestation of CF, but the most popular suggests that the altered ion concentration leads to dehydration of the airway epithelium (5). In brief, it is thought that in order to balance the flow of sodium ions into the respiratory cell epithelium when ENac is unregulated, water also flows into the cell by osmosis. As the water is drawn into the cell and out of the ASL, it depletes the volume of the ASL and exposes the lung cilia to the mucus layer. Because the cilia cannot function properly in the viscid environment, they cannot effectively clear mucus from the airways, resulting in the accumulation of a thick mucus layer that then clogs the small airways and promotes bacterial infection (5). These bacteria thrive in the thickened, nutrient-rich mucus, which shelters them from immune cells and antibiotics. Over time, these chronic infections permanently alter the lung architecture, making infections increasingly difficult to treat.

1.1 CYSTIC FIBROSIS EPIDEMIOLOGY AND PATIENT BURDEN

Despite the lethal nature of CF, the disease is surprisingly common in the Caucasian population, and is considered to be one of the most widespread life-shortening genetic diseases (6). Currently, it is estimated that around 30,000 Americans live with CF, with another 2,500 new cases occurring every year (6,7).

Cystic fibrosis usually manifests within a year of birth, but onset may be delayed until adolescence with severe complications continuing until death. Early in the disease progression, the lungs of CF patients develop thick, sticky mucus that blocks the small airways and allows for persistent bacterial infections. The resulting chronic inflammation leads to severe lung damage and lung disease, with respiratory failure accounting for roughly 85% of CF-associated mortality (7). In the pancreas, the thickened mucus builds up to block movement of digestive enzymes into

the small intestine, resulting in pancreatic damage, pancreatitis, malabsorption, poor growth, diabetes, osteoporosis and in older patients, exocrine pancreatic insufficiency (Reviewed in [8],9,10). Additionally, thickened mucus in the liver can change bile viscosity and result in cirrhosis and liver disease – another leading cause of CF-associated mortality (11).

Though recent advances in therapeutics have prolonged the average lifespan of CF patients from early childhood to nearly 40 years, they have also drastically increased the burden of treatment for adults living with CF. At minimum, patients are required to take daily pancreatic replacement enzymes, inhaled/nebulized antibiotics, and oral anti-inflammatory drugs, as well as partake in daily airway clearance regimens and vitamin therapy (12). A recent study reported that adult CF patients spend an average of 108 minutes a day fulfilling their treatment regimens, and that because of this, many patients opt not to complete all of the recommended therapies (12). Another study focusing on the financial burden to patients found that the average annual out-of-pocket costs for CF management are around $16,000USD per patient, with life-time costs exceeding $300,000USD (13). Because of the disease's severity and increasing complex and expensive treatment requirements, the goal of current research is to design new, more effective treatment options that reduce the daily burden on CF patients and increase their quality of life.

1.2 CHRONIC BACTERIAL INFECTION

In a healthy respiratory system, there exists a balance of microbiota: while the upper respiratory tract is colonized by a variety of commensal microorganisms, the lower respiratory tract contains very low levels of microorganisms, protected by the ability of the lung cilia to expel trapped bacteria in the mucus layer before reaching the lungs. However, as this mechanism is hindered in

cystic fibrotic lungs, common pathogens of the UTR—such as *Staphylococcue aureus* and *Haemophilus influenza*—are able to colonize the lungs at an early age (14). Over time, *Pseudomonas aeruginosa* (and to a lesser degree, *Burkholeria cepacia*) dominates the other pathogens to establish thick biofilms and large colonies that are able to subvert the host immune system and evade antibiotics. In fact, bacteria living in biofilms can have dramatically increased resistance to antibiotics in comparison to the same bacterial species living in planktonic conditions. Persistent infection with *P. aeruginosa* leads to chronic activation of the inflammatory response, with the ultimate consequence of severe immune-mediated tissue damage (15).

Though less common than *P. aeruginosa*, *Klebsiella pneumoniae* is also known to infect CF lungs and cause serious alveolar damage. Like *P. aeruginosa, K. pneumoniae* is a gram-negative, multidrug-resistant pathogen; however, unlike *P. aeruginosa, K. pneumoniae* can cause mortality, with a death rate as high as 50% for *Klebsiella* bacteremia and pneumonia (16). Additionally, some species of *K. pneumoniae* can produce *K. pneumoniae* carbapenemases (KPCs) – enzymes capable of inactivating carbapenem-class antibiotics, which are often used to treat MDR *P. aeruginosa* (17). As the gene responsible for conferring this ability is located on a mobile genetic element, dissemination of the KPC phenotype to other bacterial species poses a significant threat (18). Though not yet widespread, KPC-producing *P. aeruginosa* have been identified (19), and multiple studies have reported KPC-producing *K. pneumoniae* infection in CF patients (18,20). treatment options that reduce the daily burden on CF patients and increase their quality of life.

1.3 CURRENT TREATMENTS

Traditional treatments for CF-associated pulmonary infections rely on orally- and IV-administered antibiotics. Because these methods cannot directly target the lungs, the drugs must be delivered in very high doses that may result in serious side effects (21). In order to directly target the lungs and bypass some of these issues, recent research has focused on developing inhaled aerosol antibiotics. Currently, there are only two aerosol antibiotics approved for the treatment of CF in the US – TOBI® (tobramycin) and CAYSTON® (azethronam). However, while these drugs are superior to their oral and IV-counterparts, they are not without flaws. Multiple studies have shown that while inhaled drugs disperse well in unobstructed airways, they often fail to reach infection sites in obstructed airways (22-24). The thickened mucus and blocked airways characteristic of CF and other obstructive pulmonary diseases prevent uniform aerosol deposition, resulting in high local drug concentrations in the central airways and low to none in the peripheral airways (25,26). As such, these types of treatments may act to enhance drug-resistance selection, likely due to their inability to consistently deliver full therapeutic doses to infection sites (21,27).

A major hindrance to the dispersion of current inhaled antibiotic formulations –including both TOBI® and CAYSTON®--is the use of saline as a liquid carrier (28,29). Due to simple capillary forces, aerosolized droplets deposited onto the ASL will only spread if their surface tension is lower than that of the ASL (23); however, saline has a higher surface tension than the ASL, ~70dyn/cm compared to ~35-60dyn/cm (30,31). Therefore, theoretically, an aerosol liquid carrier with a surface tension lower than that of the ASL will be able to better transport drugs along the ASL and to regions of reduced ventilation.

1.4 SURFACTANTS

Surfactants are amphiphilic molecules capable of lowering the surface tension of aqueous solutions by adsorbing to liquid interfaces (32). They can be of natural origin, such as lecithin, or of synthetic origin, such as sodium dodecyl sulfate. Synthetic surfactants can be further classified as anionic, cationic, non-ionic, or zwitterionic, depending on the charge of their polar head groups. In the human lungs, natural pulmonary surfactant is required for pulmonary compliance and adsorbs to the air-water interface of alveoli to lower the surface tension during inhalation and expiration (33). Research stemming from the success of infant surfactant replacement therapy (SRT), in which exogenous pulmonary surfactant is instilled into the lungs of premature infants born with insufficient amounts, suggests that instilled natural surfactants can be used to create surface tension gradients capable of moving fluid from areas of low surface tension to areas of high surface tension (34-36). It is possible that these convective flows, termed Marangoni flows, can also be used to move drugs from areas of high surfactant concentration (low surface tension) to areas of low surfactant concentration (high surface tension), resulting in more uniform aerosolized drug spreading (37). In support of this theory, several animal studies have concluded that instilled drug delivery dispersion and/or efficacy can be increased by the addition of surfactant carriers (34,38,39). Of particular relevance to our work is a study by Veen et al., which showed that the addition of natural pulmonary surfactant to instilled tobramycin solution increased survival of mice infected with *Klebsiella pnuemoniae* (38). To date, however, little research has been conducted to investigate the possible benefits of surfactant-based drug carriers in aerosolized antibiotics.

Capstone FS-3100, the surfactant tested in this study, is a synthetic, non-ionic fluorinated surfactant that is approved for industrial uses. In contrast to natural pulmonary surfactant, FS-3100 has been specifically engineered to maximize surface tension reduction. Though no surfactant-

based nebulized drugs currently exist, evidence suggests that non-ionic surfactants are generally less toxic and hemolytic, cause less irritation to cellular surfaces, and more easily maintain near-neutral pH when compared to their anionic and cationic counterparts (reviewed in 40). The most noteworthy characteristic of non-ionic surfactants, however, is their ability to self-assemble into vesicles –termed niosomes—that are analogous to liposomes and are capable of transporting aqueous solutes and penetrating mucoid biofilms (41).

Fluorinated surfactants, or fluorosurfactants, are a special class of synthetic surfactants that have multiple fluorocarbons coating their tail groups. Unlike hydrocarbon surfactants, they are not amphiphilic, and are intrinsically much more effective at lowering surface tension (42). This quality is partly due to the high electronegativity and low polarizability of the fluorine atom, which reduces London dispersion forces (43). Additionally, because the carbon-fluorine bond is so strong, fluorosurfactants are much more chemically and thermally stable than other types of surfactants (43). Collectively, these traits make FS-3100 an ideal candidate surfactant for a self-dispersing pulmonary drug carrier.

1.5 IMAGING

The IVIS® Spectrum *in vivo* imaging system from Caliper Life Sciences is a cutting-edge optical imaging platform capable of performing noninvasive, real-time visualization of fluorescence and bioluminescence in small animals. In this study, we use the IVIS® SpectrumCT, which has the additional capacity to perform X-ray imaging and 3D small animal surface reconstruction via a high-speed microCT system. Only those features used in this study will be further discussed below.

For fluorescent optical imaging, the IVIS® system can detect and quantify all commonly used fluorophores, with the capacity to differentiate between multiple fluorescent reporters at once, as well as correct for tissue autofluorescence. A 150 Watt quartz tungsten halogen lamp provides the excitation light source, which is then fed through a filter to an optical switch that either directs the light to the top of the chamber (epi-illumination) or to the bottom of the stage (transillumination) (44). While transillumination setting allows for deeper tissue penetration and reduced autofluorescence, it uses a directed light source that only images at precise x,y locations; therefore, epi-illumination is preferred when imaging over a large area. To prevent autofluorescent signaling during epi-illumination, black paper or tape can be used to cover parts of the animal and manually block signaling. Additionally, using a fluorophore in the far-red region can help reduce autofluorescence, as animal tissue can fluoresce when excited with low-wavelength light.

To measure fluorescent signal, the user must first specify a region(s) of interest (ROI). These regions can be selected automatically by the software or manually by the user using pre-formed shapes, or drawn by the user free-hand. The software then quantifies the fluorescent signal within that area. Radiance, or emission radiance, is calculated as the "number of photons per second that leave a square centimeter of tissue and radiate into a solid angle of one steradian": (p/sec/cm^2/sr) (44). However, because the fluorescent signal detected depends not only on the fluorescence in the sample, but also on the intensity of the incident excitation light, the system must correct for this and instead displays fluorescence in radiant efficiency, or total emission radiance divided by incident excitation radiance: (p/sec/cm^2/sr)/($^{\mu}$W/cm^2) (44). In addition to total radiant efficiency, the software also displays average radiant efficiency, or the sum of the radiance inside of the ROI/number of ROI pixels; the standard deviation of the radiant efficiency; and the minimum and maximum values of the radiant efficiency within the ROI.

1.6 PRIOR RESEARCH

Extensive research by our colleagues here at the University of Pittsburgh and at Carnegie Mellon University has led to the creation of an optimized, self-dispersing, inhaled surfactant carrier formation that significantly enhances aerosolized drug spreading under very specific, laboratory conditions. With the results of their studies, we were able to build our murine model and test the candidate surfactant formulation to determine if it also increases aerosolized drug spreading *in vivo*. The following is a brief summary of their journey to determine the best candidate surfactant for use in our animal studies.

1.6.1 Preliminary data: *in vitro*

Before they could determine a candidate surfactant for our group to test, our colleagues conducted a series of preliminary *in vitro* studies investigating the post-deposition spreading of surfactant-based aerosols on complex surfaces analogous to the ASL. In their first study, surfactant/dye and saline/dye solutions were delivered via aerosol onto mucin solutions and HBE cell cultures derived from both CF and non-CF lungs (23). For every surface tested—including the cell cultures derived from CF lungs—they found substantial increases in dispersion using surfactants over saline (23). Other preliminary *in vitro* studies showed that, 1) while surfactant-induced surface tension gradients do drive initial spreading, the final spread of the formulation is determined more by the physical characteristics of the surfactant (45); and 2) SRT surfactant formulations are not ideal candidates for enhancing pulmonary drug dispersion (46). Together, these studies developed all of the experimental techniques required for the candidate surfactant screening research later on.

1.6.2 Preliminary data: *in vivo*

After reaching the above conclusions, our colleagues conducted a pilot imaging study to determine if surface tension enhanced dispersion could be measured in the cystic fibrotic lungs of 8 human patients (47). Using radiolabeled particles as a drug surrogate and a nuclear medicine gamma camera, they 1) successfully measured aerosol deposition and post-deposition spreading in the obstructed lungs, and 2) showed that, in a very small group of patients, natural pulmonary surfactant formulations increased aerosol medication dispersal.

1.6.3 Candidate surfactant studies

Armed with the preliminary *in vitro* and *in vivo* data, our colleagues performed multiple studies to "determine how carrier composition and physicochemical properties can be used to control the post-deposition spreading of inhaled medications and to develop an optimized self-dispersing aerosol carrier" (S. Garoff, T. Corcoran, and T. Przybycien, 25 February 2011, grant proposal). Through this work, they determined the ideal spreading compositions and aersolization parameters for three different classes of candidate surfactants: SRT-based phospholipid aggregate formulations (48); simple, synthetic oligomeric surfactants, such as Tyloxapol and SDS (32, 49,50); and low surface tension perfluorinated surfactants, such as FS-3100 (49). After extensively investigating all candidate surfactants, our colleagues chose Capstone FS-3100 for testing by our murine model.

2.0 SPECIFIC AIMS

Previous *in vitro* work by our colleagues has resulted in the determination of an optimal surfactant formulation that improves pulmonary drug dispersion under very specific, laboratory conditions. Because these *in vitro* methods cannot fully account for the complexities of human airway dynamics, animal studies are a necessary next step towards developing inhaled aerosolized medications. Therefore, the aim of this project is to determine if our candidate surfactant-based drug carrier formulation improves drug dispersion and efficacy in a murine model of *Klebsiella pneumoniae* infection over standard inhaled drug formulations. Additionally, these animal studies will allow us to use bacterial infection and recovery as a clinical outcome measure, which future human studies will be unable to assess.

2.1 AIM 1: ASSESS THE LETHALITY OF AEROSOLIZED *KLEBSIELLA PNEUMONIAE* IN MICE.

a. Determine the growth characteristics of *Klebsiella* strains in specified media in order to elucidate optimal harvest time for infection studies and to determine mathematical equations for bacterial concentration calculations.

b. Determine the infection characteristics and lethality of aerosolized *Klebsiella* in BL/6 mice.

c. Directly image progressing infection with bioluminescent *Klebsiella* using *in vivo* imaging methods to better elucidate disease course, if applicable.

2.2 AIM 2: DEVELOP AN IN VIVO MODEL TO CHARACTERIZE PULMONARY DRUG DISPERSION IN MICE USING FLUOROPHORES AS A DRUG SURROGATE.

a. Determine optimal method and conditions of dye solution delivery to optimize fluorescent imaging.

b. Develop method to quantify and compare drug dispersion using the IVIS® *in vivo* imaging system.

c. Apply method to determine if addition of surfactant improves drug dispersion in the lung compared to control solution.

3.0 MATERIALS AND METHODS

3.1 BIOSAFETY

All aerosol experiments were performed in a class III biological safety cabinet within the Aerobiology Suite in the University of Pittsburgh Regional Biocontainment Laboratory (RBL). As the SpectrumCT IVIS® imaging system is located in a ABSL3 suite within the RBL, all animal work was conducted at ABSL3 conditions in a class II biosafety cabinet. Powered air purifying respirators (PAPRs) were worn for respiratory protection, and Vesphene IIse (diluted 1:128, Steris Corporation, cat. #646101) was used for disinfection.

3.2 ANIMAL INFORMATION

All animal procedures were approved by the Institutional Animal Care and Use Committee (IACUC) at the University of Pittsburgh, under protocol number 14084237.

Mice: C57 BL/6 and B6 Albino mice were purchased from Charles Rivers and Jackson Labs and fed alfalfa-free chow (Envigo:2920X) upon arrival for at least one week prior to imaging to minimize autofluorescence during imaging. For temperature monitoring during infection studies, mice were implanted with temperature chips (BMDS: IPTT-300) prior to infection. For infection studies, mice were monitored at least twice daily for temperature, weight loss, and changes in behavior and appearance. Mice used in infection studies were euthanized when moribund or at study end point. All mice were euthanized by carbon dioxide intoxication followed by cervical dislocation to confirm euthanasia.

3.3 BACTERIAL STRAINS AND GROWTH CONDITIONS

Luciferase-expressing *K. pnuemoniae* strain *Kp* Xen-39 (ATCC 93A 5370) was obtained from Dr. Min Wu and the University of North Dakota. Xen-39 was originally made by Caliper Life Sciences (now part of PerkinElmer) and is specifically designed for use with their IVIS® imaging system. *K. pnuemoniae* (ATCC 43816 serotype 2) was kindly provided by Dr. Janet S. Lee (University of Pittsburgh School of Medicine).

All bacteria were stored in -80°C as 25% glycerol stocks. Overnight cultures were prepared by streaking a Luria-Bertani (LB) agar (BD Difco™, cat. #244520) plate with a small quantity of frozen bacterial stock. The plates were then incubated for 16-24 hours at 37°C. Several colonies

were then selected from each plate and re-suspended in 2.5ml of growth media. After adjusting the optical density to 0.06 to .08 at 600 nm, 0.5 ml of the bacteria solution was added to 24.5ml of growth media in a 125ml filter top flask. Cultures were incubated for 4 hours at 37°C with shaking. *Kp* Xen-39 was cultured in LB broth; ATCC 43816 was cultured in both LB broth and trypticase soy broth (TSB) (BD Difco™, cat. #211825).

3.4 FLUOROPHORES

Fluorescent carboxylic acid dye Alexa Fluor® 647 and 750 were obtained from Thermo Fischer Scientific. SPHERO™ Sky Blue fluorescent microparticles were obtained from Spherotech, Inc (Lakeforest, IL). The excitation and emission maximums for all fluorophores are summarized in Table 1.

Table 1. Excitation and Emission Maximums of Fluorophores

Fluorophore	**Excitation Maximum (nm)**	**Emission Maximum (nm)**
SPHERO™ Sky Blue microparticles	675	700
Alexa Fluor® 647 carboxylic acid dye	650	665
Alexa Fluor® 750 carboxylic acid dye	749	775

3.5 GROWTH ASSAY

Prior to any experiments, growth curves were established for both *Klebsiella* strains to determine log-phase growth. Briefly, bacterial cultures were prepared as previously described in either LB or TSB. These 25ml cultures (in 125ml filter top baffled Erlenmeyer flasks) were placed on a 200

rpm shaker at 37°C for up to six hours. At every hour starting at time zero, 300 µl of each culture were removed for measurement: 200 µl were placed in a clear 96-well plate for OD reading at 600nm; 100 µl were serially diluted out to 10e-11 and dilutions were plated in triplicate on LB plates. For luciferase-expressing *Kp* Xen-39, and additional 200 µl were removed at each hour for bioluminescent reading. Using the resulting optical density and colony-forming-unit growth curves, non-linear regression was used to determine bacterial concentration.

3.6 AEROSOLS

3.6.1 *Klebsiella* aerosols

Bacteria aerosols were performed using a Collison 3-jet nebulizer (CH Technologies, Westwood, NJ) and a rodent, whole-body chamber controlled by the AeroMP exposure system (Biaera Technologies, Hagerstown, MD). Each experiment consisted of one to five runs, ten minutes in length followed by a five-minute air wash. On the day of aerosol, 25ml *Klebsiella* cultures were harvested after 4 hours of growth in LB broth, at 37°C with shaking at 200rpm. The optical density (OD) at 600nm was taken, and then the sample was diluted to the desired starting bacterial concentration based on derived equations. Serial dilutions were then made by diluting 2.5ml of the culture in an additional 22.5ml of LB broth, out to 1:10,000 depending on the experiment. Aerosol runs proceeded from lowest bacterial concentration to highest bacterial concentration.

Aerosol samples were collected using an all-glass impinger (AGI), each prepared with 10ml of LB broth and 40 µl of antifoam. To determine aerosol concentrations, tenfold dilutions of all AGI samples were made out to 10e-7, and dilutions of all nebulizer samples out to 10e-9 using

1X Phosphate Buffered Saline (PBS). A multichannel pipette was used to "drop" 10 µl of five successive dilutions onto an LB plate, and the "drops" were then allowed to drip vertically along the plate such that no dilutions mixed. All samples were plated in triplicate and incubated overnight at 37°C. Dilutions with 10-100 colonies were counted and used to determine bacterial titers.

3.6.2 Fluorescent drug surrogate aerosols

Fluorescent drug surrogate aerosols were performed using an Aeroneb nebulizer (Aerogen) and a rodent, nose-only chamber controlled by the AeroMP exposure system. Each experiment consisted of two to six runs, ten to twenty minutes in length. 0.5 ml of SPHERO™ Sky Blue microspheres were diluted in 9.5 ml of either deionized water or 1% Capstone FS-3100 (DuPont, Wilmington, DE); or 0.5 mg of Alexa Fluor® 750 were suspended in 500 µl DMSO, then added to 19.5 ml of either deionized water or 1% FS-3100. Sham aerosols were performed first without animals to determine particle size and spray factor. Aerosol samples were collected using an AGI, each prepared with 10ml of deionized water and 40 µl of antifoam. A Next-Generation Impactor (MSP Corp., Shoreview, MN) and Aerodynamic Particle Sizer (TSI, Shoreview, MN) were used to determine aerosol particle size (Figure 1). Aerosols with animals were performed using the same parameters as sham aerosols, four to five animals at a time, with imaging immediately post aerosol completion.

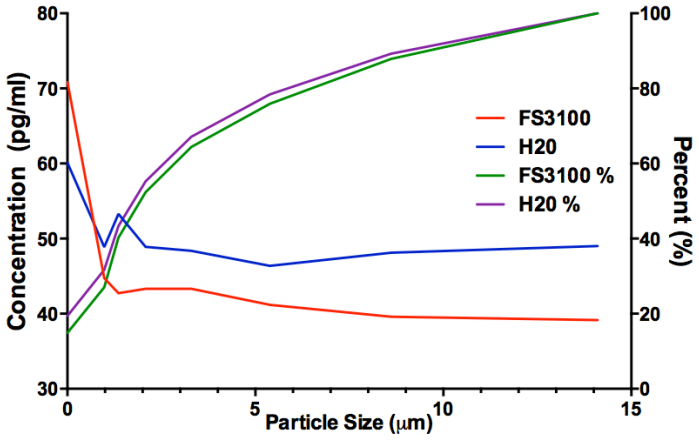

Figure 1. Particle size of aerosolized Sky Blue Microspheres and Alexa Fluor® 750

Particle size, measured as mass median aerodynamic diameter (MMAD), of Alexa Fluor® 750 diluted in both deionized water (blue/purple) and FS-3100 surfactant (red/green). Particle size is approximately the same for both water and FS-3100, about 2 µm.

3.7 IMIT INSTILLATION

Intubation-mediated intratracheal (IMIT) instillation protocol was adapted from Lawrenz, et al. (51). First, 5 mg of Alexa Fluor® 750 were suspended in 500 µl DMSO, then added to 2ml of deionized water, FS-3100, or isotonic saline for a final concentration of 2mg/ml. BL/6 mice were anesthetized using 75mg/kg ketamine and 1.0mg/kg dexmedetomidine. Only one mouse was done at a time to ensure adequate anesthesia and minimal time between delivery of dye and imaging. After mice were sedated, 10 µL of 2% of lidocaine was applied to the throat using a micropipette, and mice were allowed to rest for 5 minutes to allow lidocaine to reach full effect. At this point, mice were imaged on the IVIS® to determine pre-exposure levels of fluorescence. Next, dye/water or dye/surfactant solutions were pre-loaded into a 250 µl gas-tight precision glass syringe fitted

with a 22G long blunt needle. First, 150 µl of air were drawn up into the syringe, followed by 10, 25, or 50 µl of either dye/water or dye/surfactant, followed by additional air to equal 200 µl in total. The mouse was placed on the intubation platform and secured by hooking its incisors with an O-ring to the intubation platform. The platform was then raised to a 45° incline. Using a cotton applicator, the tongue was retracted and a wire-guided, 20G 1" catheter was inserted through the mouth to a 10 mm depth into the trachea. To confirm successful intubation, a 1/16" tubing containing 20 µl of Coomassie Brilliant Blue dye was secured to the catheter; if the dye migrated rapidly back and forth (in response to the animal's breathing), intubation was successful. If successful intubation could not be confirmed, no more than two more attempts were made in a single session to prevent causing trauma to the mouse. Finally, the glass syringe was inserted through the catheter to 1" depth, and the contents slowly dispensed into the lungs in a single fluid motion. The needle and catheter were then removed and mice imaged immediately on the IVIS®.

3.8 IVIS IMAGING

All imaging took place within the RBL rodent suit under ABSL-3 conditions due to the location of the IVIS®. Mice imaged post-aerosol were first anesthetized using an isoflurane/oxygen, with continued dosing during imaging; mice imaged post-IMIT were only given a light isoflurane dose during imaging to sustain ketamine/dexmedetomidine anesthesia. Using the excitation and emission wavelengths that best complemented each reagent, the mouse whole body was then imaged on an In Vivo Imaging System SpectrumCT (IVIS®; PerkinElmer) to measure fluorescent signal. All image reconstruction and imaging analysis was done on a separate computer using Living Image® 4.5.2 software (Perkin Elmer) that is designed for use with the IVIS®. In most

cases, only the IVIS® 2D imaging functions were used; however, several animals also underwent 3D fluorescence imaging tomography (FLIT) to confirm dye localization. In the case of FLIT, animals' abdomens were shaved prior to imaging to increase FLIT signal, as recommended by PerkinElmer.

3.9 REGION OF INTEREST ANALYSIS

Using the Living Image 4.5.2 software, two oval regions of interest (ROI) were drawn around the mouse lungs to measure total and central lung fluorescence (Figure 2). Total lung fluorescence was measured by the larger, outer oval region; central lung fluorescence was measured by the smaller, inner oval region; the peripheral fluorescence was calculated as the difference between the two regions. The ratio of peripheral fluorescence to total fluorescence (P/T) was then used to determine the extent of dispersion from central to peripheral lung regions. Within the context of this study, the terms "central" and "peripheral" are only used to describe the 2D regions illustrated in Figure 2, and do not refer to any particular anatomical regions of the lungs. The central region corresponds roughly to the dye solution deposition site, and the peripheral region to those sites farthest away from the initial deposition site. Fluorescence was measured by radiant efficiency, in units $(p/sec/cm^2/sr)/(\mu W/cm^2)$. ROI size and shape were maintained across all images (Table 2), and all images were adjusted to the same fluorescent scale to ensure accurate visual comparison.

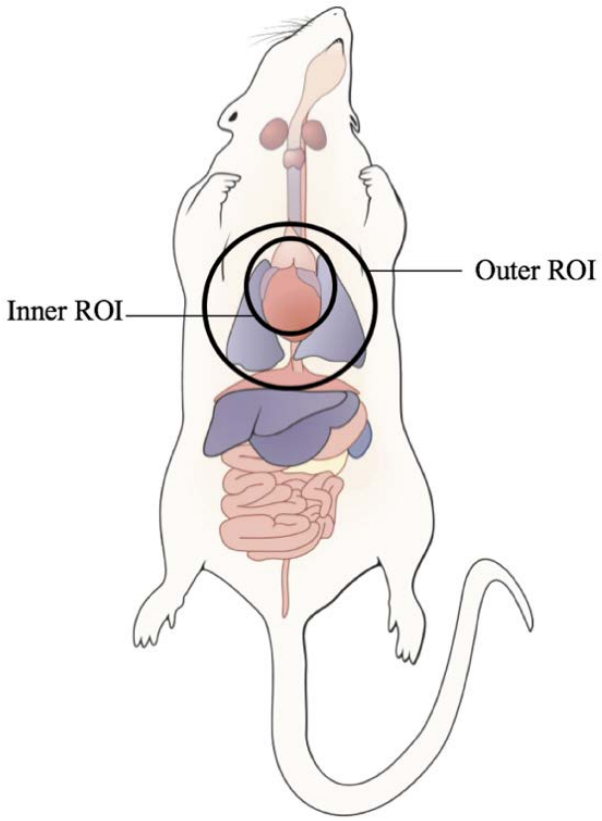

Figure 2. Region of Interest (ROI) Diagram

Location of the two ROI drawn around mouse lungs. Total lung fluorescence is measured by the outer ROI, which encompasses the entire lung region. Central lung fluorescence is measured by the inner ROI, which encompasses only the central airways. Peripheral lung fluorescence is then calculated by subtracting the central fluorescence from the total fluorescence.

Table 2. ROI circumference and total area, in pixels

	Circumference	**Area**
Outer ROI	408	8.403e04
Inner ROI	131	2.611e04

3.10 STATISTICAL ANALYSIS

GraphPad Prism® 6 was used to create all graphs and equations, and to perform two-sided T-tests comparing the P/T ratios between water and surfactant treatment groups. $P<0.05$ was considered statistically significant. Non-linear regression analysis was used to create the bacterial concentration equations due to the non-linear relationship between OD600 and bacterial concentration.

4.0 RESULTS

4.1 AIM 1: ASSESS THE LETHALITY OF AEROSOLIZED *KLEBSIELLA PNUEMONIAE* IN MICE

Before beginning any experiments, we first needed to determine the growth characteristics of our *Klebsiella pneumoniae* (*Kp*) strains (Figure 3). At every hour out to six hours, the optical density was recorded at 600 nm (Figure 3A,B). For the luciferase-expressing *Kp* Xen-39 strain, the hourly luminescence was also recorded (Figure 3C). However, for reasons that will be discussed later, we eventually had to replace the luminescent *Kp* Xen-39 strain with the highly pathogenic, *Kp* ATCC 43816 strain. Because we had been growing *Kp* Xen-39 in Luria-Bertaini (LB) broth, but trypticase soy broth (TSB) was recommended for ATCC 43816, we decided to compare the growth rates of the ATCC 43816 in both media (Figure 3B). Though the bacteria did seem to grow slightly better in TSB, we did not find the difference to be significant. Therefore, even though all initial experiments were performed with *Kp* Xen-39, we felt comfortable moving forward with the ATCC 43816 strain.

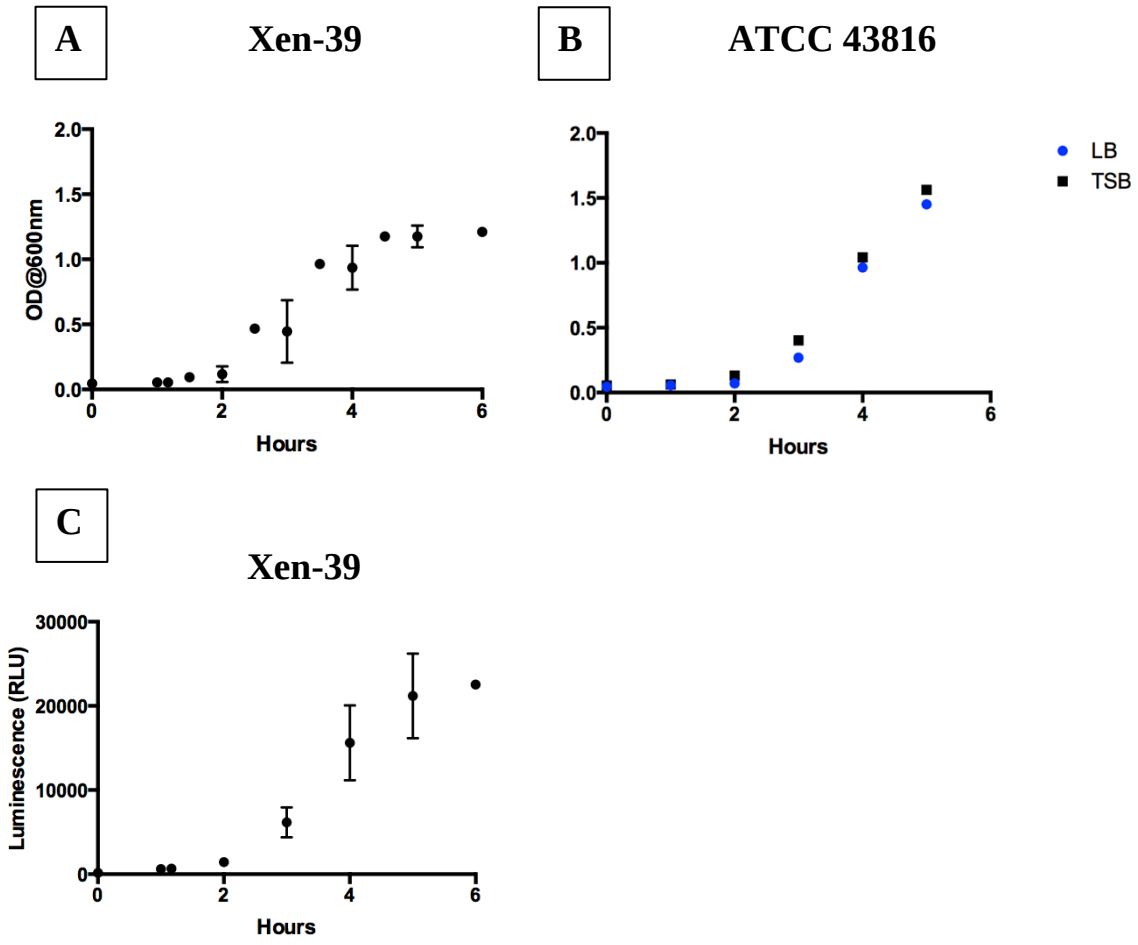

Figure 3. Growth characteristics of *Klebsiella pneumoniae* strains

Optical density at 600nm vs time in hours: (A) Two replicates of Xen-39 grown in LB broth; (B) ATCC 43816 grown in LB broth (blue) and TSB (black). (C) Luminescence in Relative Light Units (RLU) vs time in hours

While performing each growth curve, I also plated serial dilutions of the hourly samples, and used those to calculate colony-forming-units per milliliter at each time point (CFUs). I then used non-linear regression analysis to compare optical density to measured cell counts, and derived an equation to calculate concentration based on optical density (Figure 4, Table 3). These equations were used in later aerosol exposures to determine the ideal initial bacterial concentrations to deliver a specific inhaled dose.

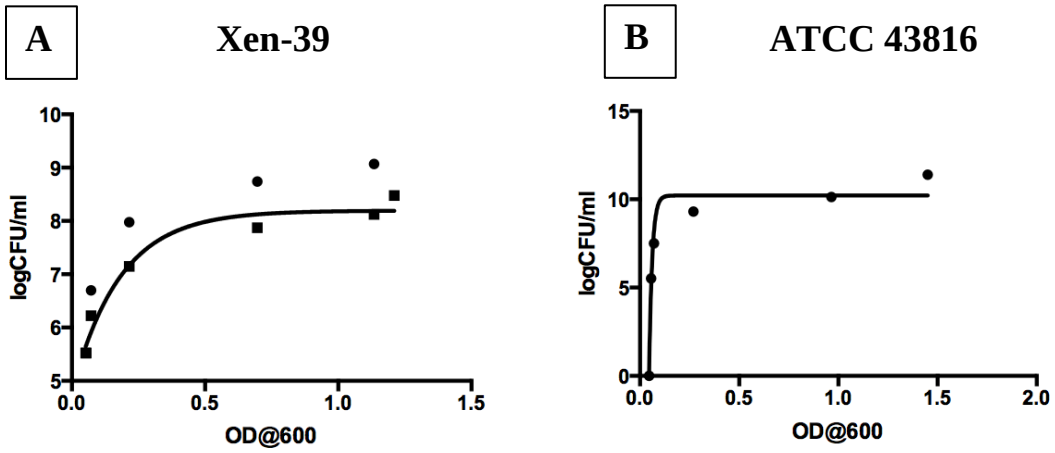

Figure 4. Calibration curve to convert optical density at 600nm to bacterial concentration in CFU/ml

(A) Xen-39 and (B) ATCC 43816. Logarithmic transformation was performed to best fit the data.

Table 3. Equations generated from calibration curve

***Kp* Strain**	**Equation**
Xen-39	Y= -4920 + 4928.19 / (1+10^ ((-1.307 – X)*2.417))
ATCC 43816	Y = -23387 + 23397.22 / (1+10^ ((-0.07382 – X)*28.10))

Y = Log_{10}(bacterial concentration in CFU/ml); X = OD@600nm

In order to determine the lethality of the *Kp* Xen-39 strain, BL/6 mice were exposed to increasing log10 doses of aerosolized *Kp* Xen-39 using a Collison 3-jet nebulizer and a rodent, whole-body exposure chamber. Fifty mice were infected in five groups of ten, with Group 1 representing the lowest dose of *Kp* and Group 5 representing the highest dose. Starting concentration in the nebulizer was approximated using the standard curve calculated for *Kp* Xen-39, and final inhaled doses were calculated by plating serial dilutions of aerosol samples and then adjusting for spray factor. Mice were then monitored twice daily for seven days post-exposure for changes in weight, temperature, natural and provoked behavior, and appearance. Unfortunately, none of the groups showed significant weight loss during the monitoring period (Figure 5A), nor did they show any other signs of illness (data not shown). Given that *Kp* Xen-39 expresses luciferase and was developed for imaging with the IVIS®, we attempted to directly visualize the *Kp* in the mouse lungs. Three mice from each infection group were imaged in the IVIS® on days 0, 1, 2 and 4 post-infection; however, no luminescence was measured at any time point (data not shown). To confirm these results, we performed a smaller, but similar experiment using only five mice and a very high dose of *Kp* Xen-39, 1.5 x 10^8 CFUs, and still did not observe any signs of illness or luminescence (data not shown).

Given that *Kp* Xen-39 did not result in observable illness or luminescence, we decided to switch to *Kp* ATCC 43816 – a known pathogenic strain in BL/6 mice – based on the recommendation of Dr. Janet Lee (who also provided the strain). After a preliminary test using only five mice and a dose of 9×10^5 CFU resulted in the death of all five mice within 72 hours (data not shown), we proceeded with another lethality assay similar to the one performed with *Kp* Xen-39. Twenty mice were split into four groups of five and infected with increasing log10 doses of aerosolized ATCC 43816 and monitored for six days post-infection, by which time all mice had succumbed to illness (Figure 5B). The initial dose was calculated using the standard curve, and all final doses by serial dilution plating of the nebulizer samples.

The euthanasia criteria employed was based on a combination of factors meant to assess febrile illness and weight loss in mice (Appendix A). A combined score of 16 or higher must result in euthanasia, and any animal showing a sustained temperature below 34°C (2 or more consecutive readings) or weight loss above 20% must also be euthanized promptly. Because none of the mice lost a significant amount of weight but all developed severe hypothermia (temperature below 34^0C), time of euthanasia was determined by temperature in combination with significantly subdued behavior (Figure 5C).

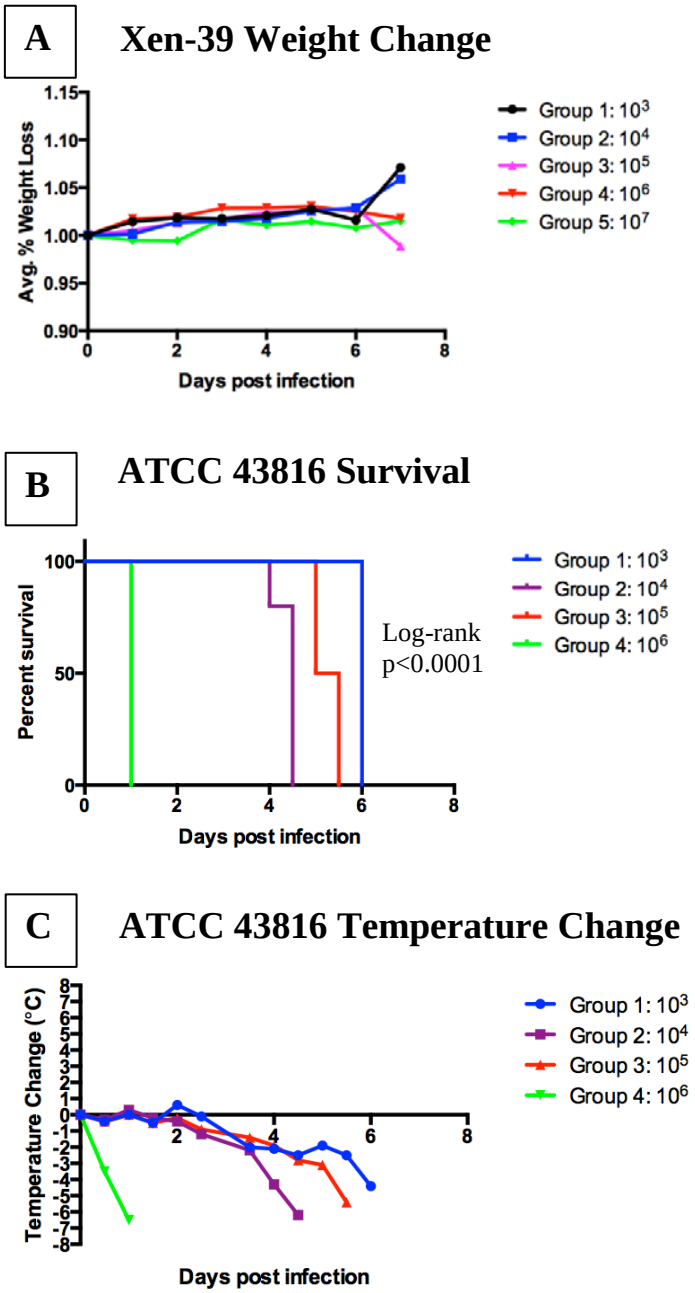

Figure 5. Lethality Assay

Fifty BL/6 mice were infected via aerosol with increasing log10 doses of *Kp* Xen-39. Animals were monitored twice-daily for seven days post-infection for signs of illness, including weight change (A). Inhaled doses: Group 1 = 5.05 x 10^3 CFU; 2 = 4.56 x10^4 CFU; 3 = 6.14 x 10^5 CFU; G 4 = 5.67 x 10^6 CFU; 5 = 3.87 x 10^7 CFU. Twenty BL/6 mice were infected via aerosol with increasing log10 doses of Kp ATCC 43816 and monitored twice-daily for six days post-infection, at which point all animals succumbed to illness (B). Inhaled doses: Group 1 = 6.06 x 10^3 CFU; 2 = 6.00 x 10^4 CFU; 3 = 3.03 x 10^5 CFU; 4 = 4.33 x 10^6 CFU. Temperature change (C) was the only defining characteristic of illness.

4.2 AIM 2: DEVELOP AN IN VIVO MODEL TO CHARACTERIZE PULMONARY DRUG DISPERSION IN MICE USING FLUOROPHORES AS A DRUG SURROGATE

4.2.1 Dispersion assay: Aerosolized microspheres

In the first attempt to visualize lung dispersion, two different sizes of Spherotech SPHERO™ Sky Blue fluorescent microspheres in the nanometer range were delivered via aerosol with a vibrating mesh nebulizer. Prior to animal experiments, microspheres were mixed with either deionized water or Capstone FS-3100 surfactant to determine aerosol characteristics in the presence of surfactant (data not shown). Aerosol particle size was determined using a Next-Generation Impactor with direct sampling from the aerosol chamber.

In the first animal experiment, four BL/6 mice were exposed to aerosolized Sky Blue microspheres in size 0.1-0.3 μm mixed with surfactant or water, and then imaged immediately after using the IVIS® (Figure 6). Because the Sky Blue microspheres are not one of the 99 pre-programmed fluorescent reporters in the Living Image 4.5.2 software database, we had to manually set the excitation and emission peak wavelengths for the software to read. Based on the data provided by Spherotech, we chose an excitation peak around 675nm and an emission peak around 700nm. After two separate attempts using the same conditions resulted in no measurable fluorescence, we concluded that the skin and fur could be obscuring the signal and decided to image the lungs directly. The mice were euthanized promptly, and imaged with their chest cavities opened and lungs exposed; the lungs were then removed and imaged separately (data not shown). As we were still unable to measure any fluorescence, we considered the possibility that the microspheres were clogging the nebulizer and decided to perform another two aerosols using a smaller size of Sky Blue microspheres, 0.04-0.09 μm (data not shown). After reiterating the same

process only to achieve the same results, we concluded that the fluorescent microspheres were not the ideal drug surrogate for this study and considered other fluorophores.

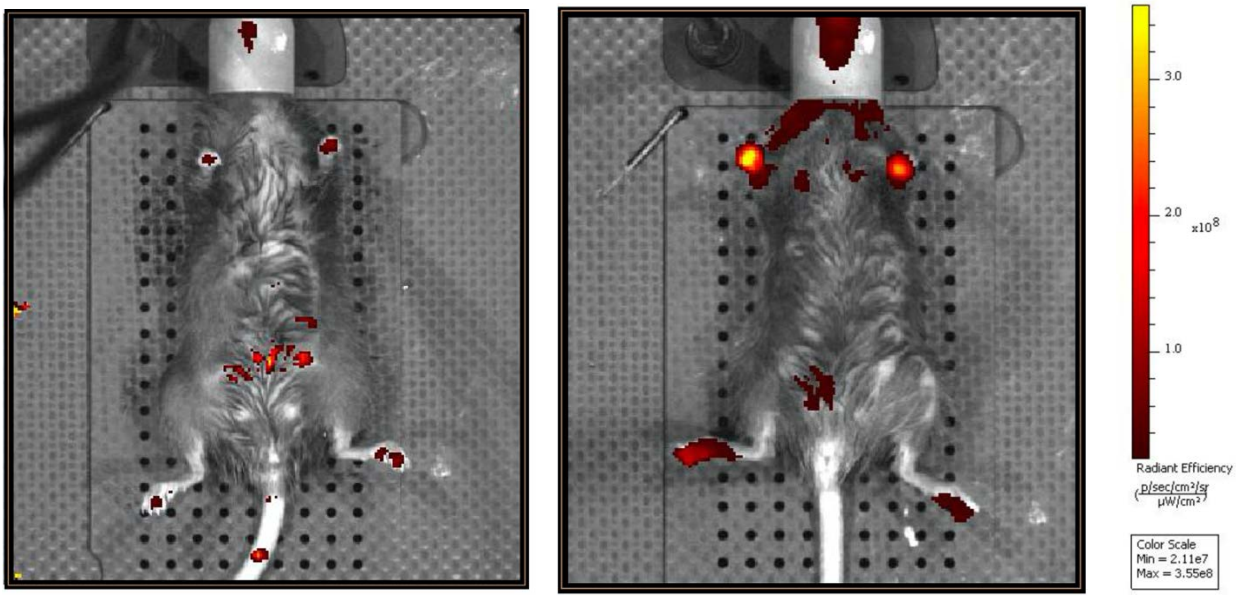

Figure 6. Representative IVIS® images

Mouse exposed to aerosolized Sky Blue microspheres, size = 0.1-0.3 µm diluted in water (right), and Alexa Fluor® 750 diluted in water (left). Red = fluorescent signal.

4.2.2 Dispersion assay: Aerosolized fluorescent dye

In a second attempt to visualize lung dispersion, the fluorescent microspheres were replaced with Alexa Fluor® 750 carboxylic acid dye. Before the initiation of this study, our group had attempted to visualize lung dispersion using Alexa Fluor® 647 with little success; however, because photon scattering is reduced at longer wavelengths and Alexa Fluor® 750 is farther red-shifted, we hypothesized that it would result in more sensitive fluorescent measurements than the Alexa Fluor® 647.

As with the microspheres, the Alexa Fluor® 750 dye was first mixed with either deionized water or Capstone FS-3100 surfactant to determine aerosol characteristics in the presence of surfactant (Figure 1). Once it was confirmed that the addition of surfactant did not alter the particle size, we continued with animal experiments.

We performed a total of three aerosols with four BL/6 mice each; in each experiment, two mice were exposed to the water/dye solution, and two were exposed to the surfactant/dye solution. Immediately following exposure, mice were anesthetized and imaged on the IVIS® using the pre-programmed Living Image software emission and excitation peak wavelengths for Alexa Fluor® 750: 775nm and 800nm respectively. Just as with the microspheres, little or no fluorescence was observed in the lungs in any animal exposed (Figure 6B); even when the lungs were removed and imaged separately, no difference in fluorescence was observed between groups (data not shown). Given that the whole body images only showed fluorescence in the upper neck and throat region, we concluded that either 1) aerosolization using the capabilities we have available cannot deliver a sufficient volume of the solution deep enough into the lungs to produce a measurable signal with the IVIS®, or 2) the time difference between exposure and imaging (between 20-30 minutes) due to transportation of the animals between different suits could be dampening the fluorescent signal.

4.2.3 Dispersion assay: Intubation-mediated intratracheal instillation (IMIT)

After multiple unsuccessful attempts to deliver the dye solution via aerosol, we decided to instead adopt an intubation-mediated intratracheal (IMIT) instillation method of delivery. In brief, mice are anesthetized using ketamine/dexmedetomidine, and placed on a platform raised to a 45° angle. A catheter fitted to a guide-wire is then inserted into the trachea; once the catheter is in place, the guide-wire is removed and replaced with a 20G blunt-end syringe needle that is loaded with 150µl

of air + 10-50µl of water/dye or surfactant/dye. In order to validate the procedure, several test runs were performed using Coomassie Brilliant Blue dye diluted in water. Mice were euthanized immediately after delivery and their lungs removed to confirm the presence of dye. Initially, we had intended to anesthetize mice using isoflurane alone; however, we realized during the test runs that the procedure was more time-intensive than the isoflurane allowed, so we altered the procedure to include anesthesia via ketamine/dexmedetomidine.

In the first attempts using the IMIT procedure, we instilled 150µl of air + 50µl of dye/water or dye/surfactant solution into C57 BL/6 mice, and then allowed the mice to rest on the intubation platform at 45^{o} for five minutes post-delivery before imaging (Figure 7). Due to an inexperience with the technique, only two out of twelve attempts were successful: one with water/dye solution, one with surfactant/dye solution. At this point in our study, we had not yet developed our model for measuring dye dispersion, so instead we measured the total lung fluorescence and the standard deviation of the lung fluorescence using the IVIS® ROI tool. (Table 4). Between the two groups, the standard deviation of the fluorescence intensity in the mouse instilled with water/dye solution was roughly 3X that of the standard deviation of the fluorescence intensity in the mouse instilled with surfactant/dye solution. Additionally, the range in fluorescence intensity in the mouse instilled with the water/dye solution was roughly 4X higher than the range of fluorescence intensity in the mouse instilled with surfactant/dye solution. Taken together, we believe this shows less uniformity in dye dispersion in the lungs of the mouse instilled with the water solution.

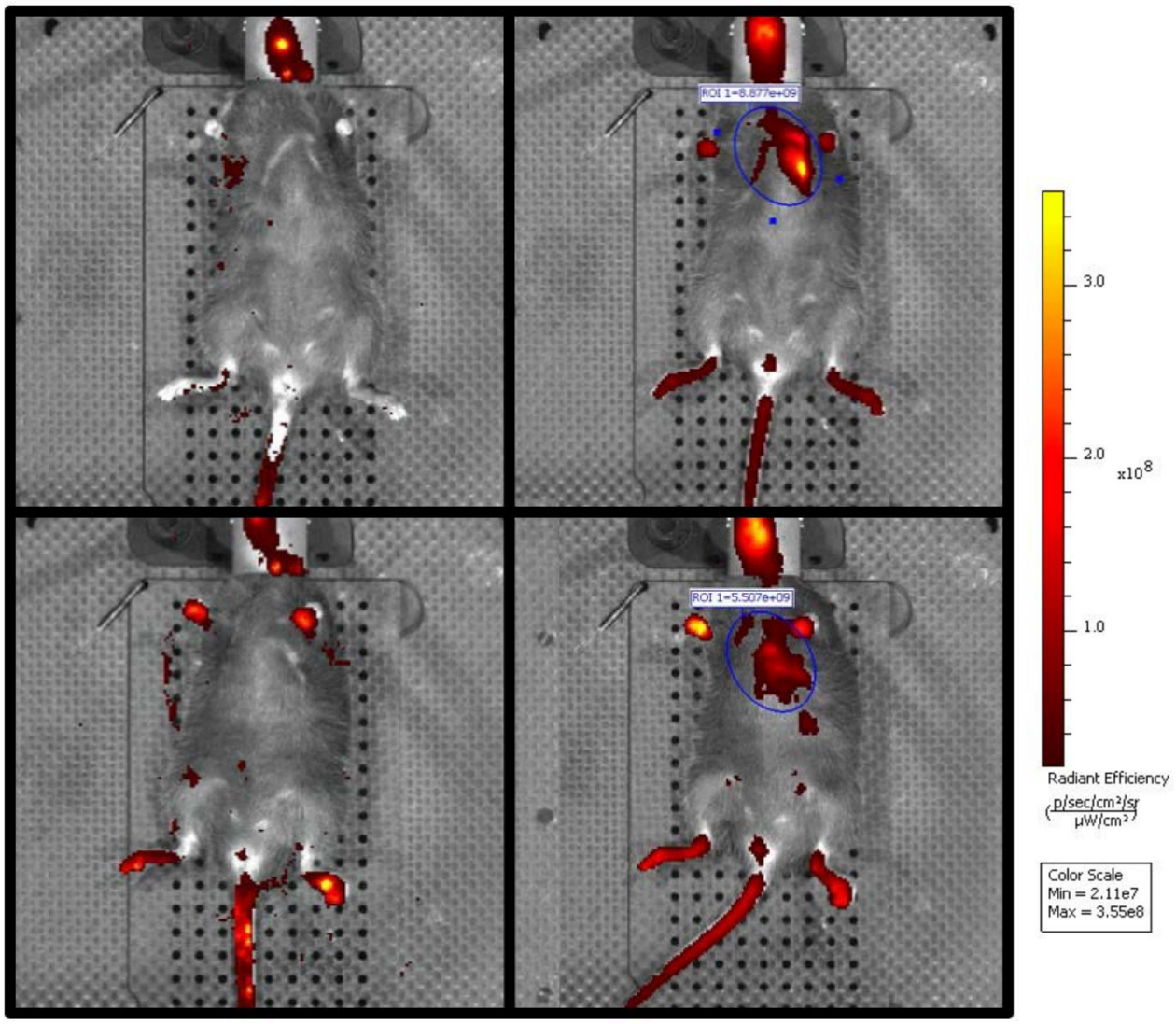

Figure 7. IMIT instillation with 50 µl of Alexa Fluor® 750 fluorescent dye solution

Top: Before and 5 minutes after instillation with 50 µl of Alexa Fluor® 750 + water. *Bottom*: Before and after instillation with 50 µl of Alexa Fluor® 750 + FS-3100. ROI = Region of Interest (blue), indicates total fluorescence within region. All imaging conditions were the same in all images.

Table 4. ROI fluorescence measurements of mice instilled with 50 µl of Alexa Fluor® 750 fluorescent dye solution

	Total Rad. Efficiency	Avg. Rad. Efficiency	Stdev Rad. Efficiency	Range Rad. Efficiency
Water	8.88e09	2.16e08	3.19e08	2.26e09
FS-3100	5.51e09	1.34e08	1.20e08	6.09e08

Radiant Efficiency = $(p/sec/cm^2/sr)/(^{\mu}W/cm^2)$

After discussing this data with our colleagues, it was suggested that resting the mice on the incline for five minutes post-instillation before imaging could be altering our results by allowing gravity to increase dispersion. It was also suggested that 50 µl of dye solution may be flooding the lungs and preventing dispersion. With this advice, we altered our procedure to image the next set of C57 BL/6 mice immediately post-instillation, and reduced the instillation amount from 50µl to 25µl of dye solution (Figure 8). CT scans of every other mouse instilled were performed using the IVIS® to confirm the localization of the fluorescent signal within the lung region (Figure 9). In the mice instilled with water/dye solution (n=10), there are more concentrated, brighter spots of fluorescence than in the mice instilled with surfactant/dye (n=11), suggesting less uniform distribution of the dye when diluted in water. In an attempt to quantify this difference, we developed a system to measure the fluorescence in the peripheral regions of the lungs using two different ROI for each mouse as illustrated in Figure 2. We then calculated the ratio of peripheral fluorescence to total fluorescence (P/T) to index the extent of pulmonary dispersion (Table 5). A two-sided T-test comparing the P/T ratios of mice instilled with water/dye to mice instilled with surfactant/dye resulted in a p-value of 0.0824. Though these results are not statistically significant, they do suggest that FS-3100 increases pulmonary drug dispersion.

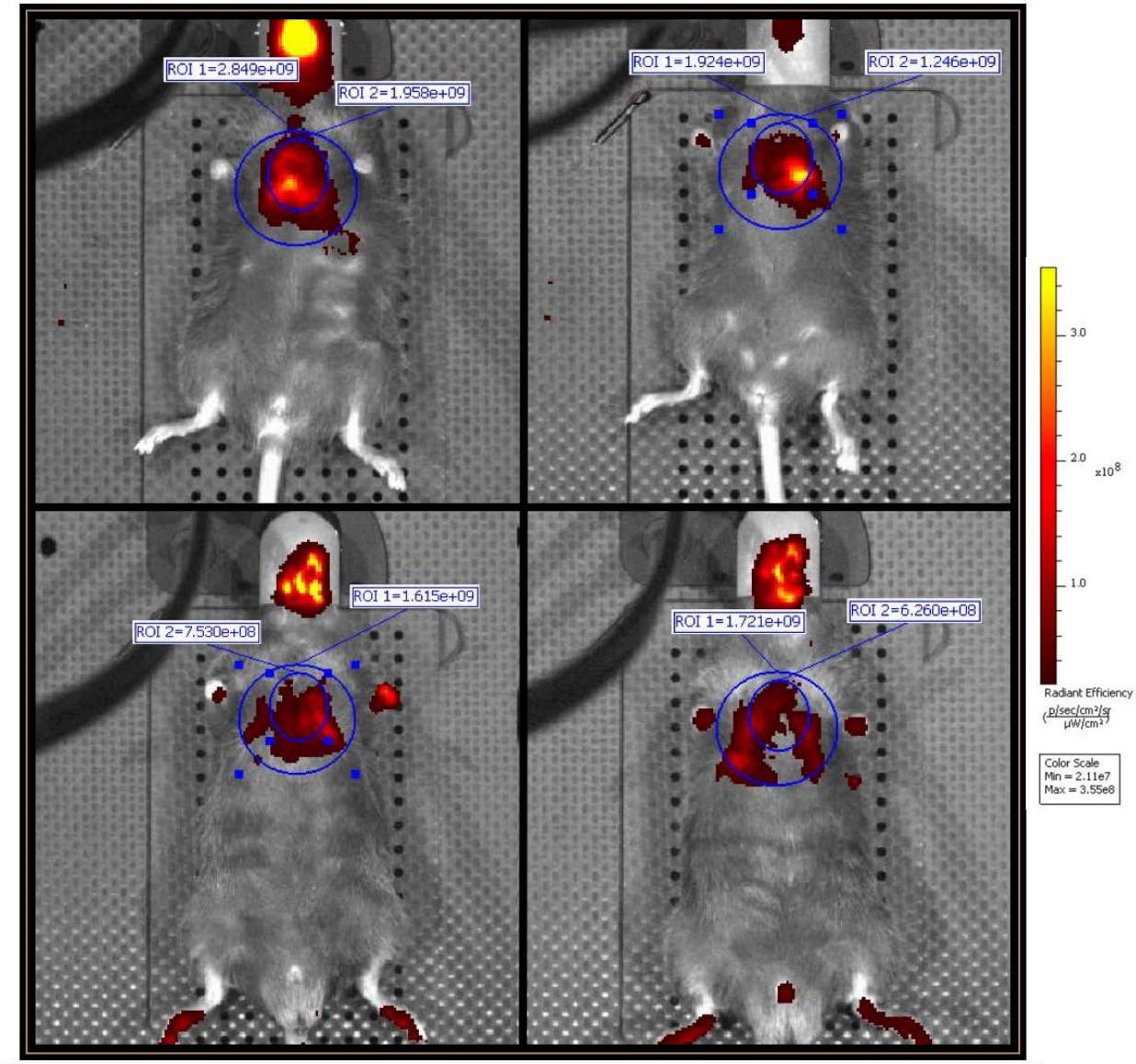

Figure 8. IMIT instillation with 25 µl of Alexa Fluor® 750 fluorescent dye solution

Top: Representative images of mice instilled with 25 µl of Alexa Fluor® 750 + water (n=10). *Bottom*: Representative images of mice instilled with 25 µl of Alexa Fluor® 750 + FS-3100 (n=11). All imaging conditions were the same in all images.

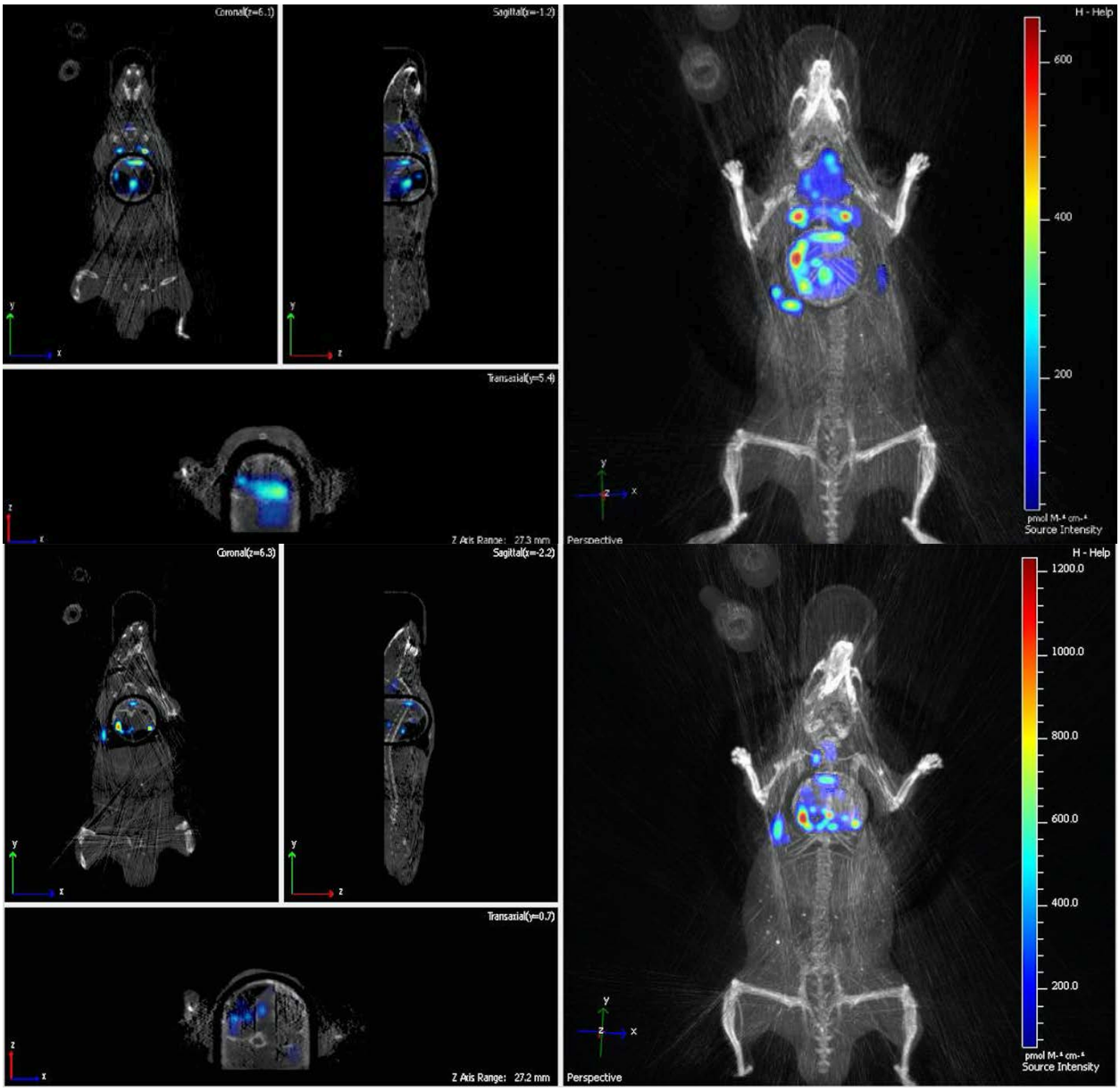

Figure 9. 3D fluorescence imaging tomography (FLIT) of mice instilled with 25 µl of Alexa Fluor® 750 dye solution

Top: Representative CT image of mouse instilled with 25 µl of Alexa Fluor® + water. *Bottom:* Representative CT image of mouse instilled with 25 µl of Alexa Fluor® + FS-3100.

Table 5. Fluorescence by region and P/T ratios of mice instilled with 25 µl of Alexa Fluor® 750 dye solution

	Total	Central	Peripheral	P/T Ratio
Water	1.92e09	1.25e09	6.78e08	35.24
Water	2.04e09	1.02e09	1.01e09	49.71
Water	3.25e09	2.24e09	1.02e09	31.31
Water	1.39e09	6.50e08	7.36e08	53.07
Water	7.76e08	3.29e08	4.48e08	57.66
Water	1.27e09	5.85e08	6.81e08	53.81
Water	9.88e08	4.57e08	5.31e08	53.70
Water	1.56e09	7.67e08	7.94e08	50.86
Water	2.85e09	1.96e08	8.91e08	31.27
Water	2.00e09	1.18e08	8.18e08	41.00
FS-3100	3.43e09	1.73e09	1.17e09	49.77
FS-3100	3.56e09	2.17e09	1.38e09	38.87
FS-3100	1.72e09	6.26e08	1.10e09	63.63
FS-3100	1.62e09	7.53e08	8.62e08	53.37
FS-3100	1.64e09	9.77e08	6.60e08	40.29
FS-3100	1.79e09	7.78e08	1.02e09	56.64
FS-3100	1.45e09	5.96e08	8.49e08	58.75
FS-3100	3.25e09	1.63e09	1.63e09	50.00
FS-3100	2.19e09	9.85e08	1.20e09	54.94
FS-3100	3.65e09	1.39e09	2.26e09	61.98
FS-3100	3.16e09	1.50e09	1.66e09	52.52

Lung fluorescence measured in radiant efficiency, units (p/sec/cm^2/sr)/(µW/cm^2).

According to PerkinElmer, albino mice and nude mice are preferred for imaging with the IVIS® over black mice, as the black fur increases light scatter. Therefore, in an attempt to increase fluorescent signal, we performed the same procedure as above with eight B6 Albino mice. However, as the entire animal fluoresced bright red, we were unable to differentiate any signal in the lungs from the rest of the body (data not shown).

Concerned that we were still flooding the mouse lungs with a 25 µl dose of dye solution, we lowered the dose to 10 µl of solution (Figure 10). Instilling such a small amount of liquid proved challenging, and many attempts resulted in little to no fluorescence in the lungs of the mice. CT scans of every other mouse instilled were performed using the IVIS® to confirm the localization of the fluorescent signal within the lung region (Figure 11). Only eight out of thirty-two attempts resulted in measureable fluorescence, and a two-sided T-test comparing the P/T ratios of these eight subjects resulted in a non-significant p-value of 0.2597 (Table 6).

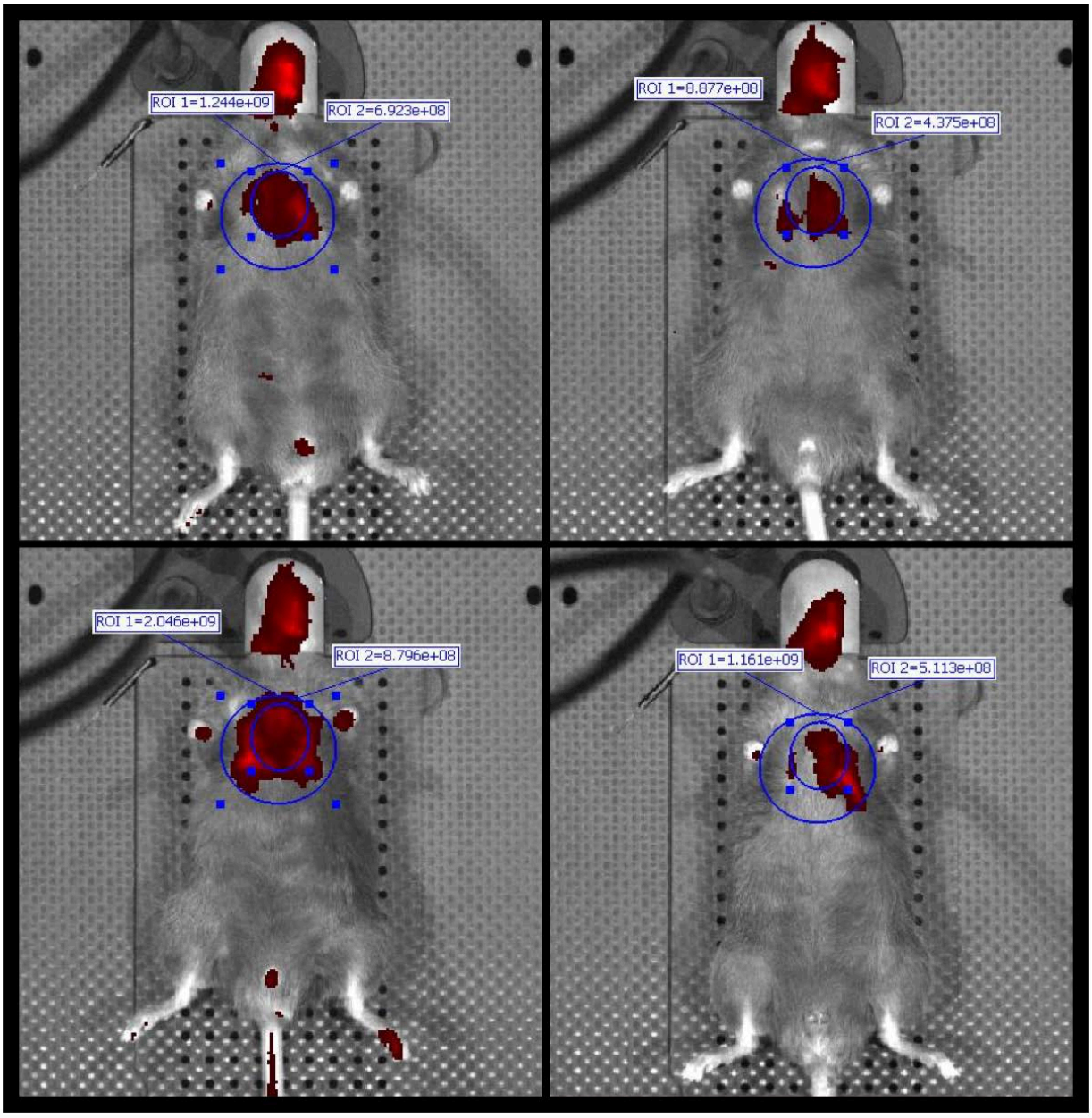

Figure 10. IMIT instillation with 10 µl of Alexa Fluor® 750 fluorescent dye solution

Top: Representative images of mice instilled with 10 µl of Alexa Fluor® 750 + water (n=3). *Bottom*: Representative images of mice instilled with 10 µl of Alexa Fluor® 750 + FS-3100 (n=5). All imaging conditions were the same in all images.

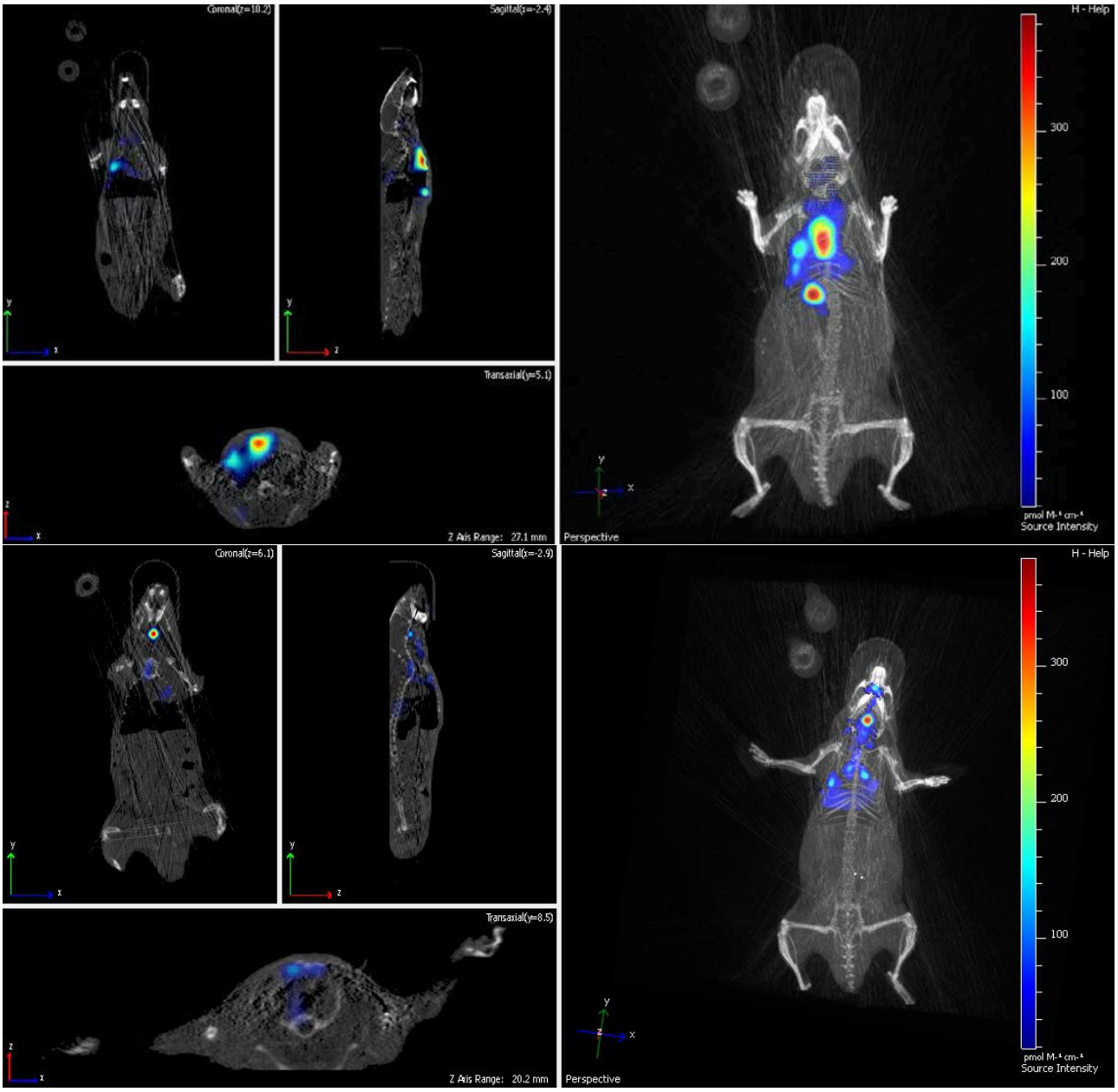

Figure 11. 3D fluorescence imaging tomography (FLIT) of mice instilled with 10 µl of Alexa Fluor® 750 dye solution

Top: Representative CT image of mouse instilled with 10 µl of Alexa Fluor® + water. *Bottom:* Representative CT image of mouse instilled with 10 µl of Alexa Fluor® + FS-3100.

Table 6. Fluorescence by region and P/T ratios of mice instilled with 10 µl of Alexa Fluor® 750 dye solution

	Total	Central	Peripheral	P/T Ratio
Water	6.23e08	2.82e08	3.42e08	58.81
Water	1.24e09	6.92e08	5.52e08	44.35
Water	8.88e08	4.38e08	4.50e08	50.71
FS-3100	1.19e09	5.88e08	6.04e08	50.65
FS-3100	1.09e09	5.61e08	5.24e08	48.31
FS-3100	1.10e09	4.68e08	6.29e08	57.32
FS-3100	2.05e09	8.80e08	1.17e09	57.01
FS-3100	7.65e08	2.48e08	5.17e08	67.60

Lung fluorescence measured in radiant efficiency, units (p/sec/cm^2/sr)/($^{\mu}$W/cm^2)

Throughout our study, water was used as the control drug carrier because the surfactant, FS-3100, is diluted in water. However, a more clinically-relevant control carrier would be saline, as that is what most aerosolized drugs are diluted in. In our last experiment, we instilled one mouse with 25 µl of saline/dye solution and calculated the P/T ratio (Table 7). Though one mouse is not enough to make a statistical comparison, a visual assessment reveals a single, concentrated region of fluorescence similar to that seen in mice instilled with 25 µl of water/dye solution (Figure 12). In the future, we will perform experiments using both saline and water as control carriers.

Table 7. Fluorescence by region and P/T ratio of mouse instilled with 25 µl of Alexa Fluor® 750 dye diluted in isotonic saline

	Total Lung	Central Lung	Peripheral Lung	P/T Ratio
Saline	3.41e09	1.64e09	1.78e09	52.10

Lung fluorescence measured in radiant efficiency, units (p/sec/cm^2/sr)/(µW/cm^2)

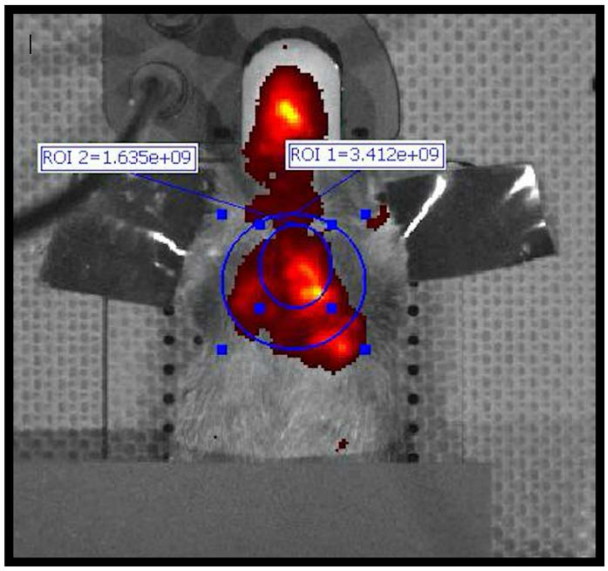

Figure 12. IMIT instillation with 25 µl of Alexa Fluor® 750 fluorescent dye diluted in isotonic saline

Black paper and tape were used to reduce autofluorescence.

Given the very small sample sizes from both sets of mice instilled with different amounts of dye solution, we combined the P/T data from all twenty-nine successfully instilled mice (not including the two instilled with 50 µl of dye). The p-value from the two-sided T-test comparing the combined P/T ratios, p=0.0287, is statistically significant and supports our hypothesis that FS-3100 increases pulmonary dispersion in a murine model.

5.0 DISCUSSION

The development of inhaled aerosol antibiotics has transformed the management of cystic fibrosis-related pulmonary infections. Aerosol antibiotics can deliver high local concentrations of drugs into the airways to directly target the sites of infection and reduce systemic toxicity. However, the efficacy of these drugs depends on their ability to deposit and spread in obstructed airways, and to do so in high enough doses to overcome the resistance mechanisms of the colonized bacteria. In order to enhance aerosolized drug spreading and efficacy, we propose using lipid surfactants as drug carriers. Saline, the current standard carrier, has a surface tension much higher than that of the airway surface liquid, and we believe this prevents its ability to fully disperse aerosolized drugs in the airways. Research associated with surfactant replacement therapies have hinted that instilled surfactants can be used to create surface tension gradients capable of driving pulmonary drug dispersion, but so far little work has been done to translate this into an inhaled antibiotic. With this in mind, we set out to determine if lipid surfactants can indeed increase pulmonary drug dispersion and efficacy in a murine model.

In order to develop a model to characterize pulmonary drug dispersion, we first needed to characterize murine bacterial pneumonia so that we can eventually perform surfactant-augmented antibiotic treatment studies. We chose to use a *Klebsiella pneumoniae* model because the *Klebsiella* model has been used in previous murine studies of surfactant-enhanced tobramycin delivery (38).

Initially, we had planned to use a bioluminescent strain of *Klebsiella*, Xen-39, for all of our bacteria experiments, believing that we would be able to directly image the bacterial infection in

the mouse lungs using the bioluminescent function of the IVIS®. However, not only were we unable to measure any luminescence *in vivo*, we were also unable to deliver a lethal dose to the mice using aerosolization. We were surprised by these results, given that a recent paper published by Tan et al. reported significant Xen-39 lethality and bioluminescence in C57BL/6 mice with an intranasally instilled dose of 10e5 CFUs (52). A literature review revealed several, older studies that reported significantly reduced virulence of some *Klebsiella pneumoniae* strains when aerosolized versus when administered by other routes of infection (53-56). Though none of these studies gave a reason for these findings, it is possible that some strains of *Klebsiella pneumoniae* are rendered less infectious when aerosolized, and that our Xen-39 is one of them. In order for a pathogen to be infectious via aerosol, it must 1) be able to withstand the harsh aerosolization conditions, and 2) remain infectious while airborne. *Klebsiella* is a gram-negative bacteria enveloped in a polysaccharide capsule, where it contains many of its virulence factors, including LPS and capsular antigens. Given that the different serotypes of *Klebseilla* vary significantly in the size and composition of their capsular polysaccharides (16), it could be that certain serotypes – of which Xen-39 may belong – are more susceptible to severe damage during aerosolization. It is also possible that the Xen-39 we acquired had simply been passaged too many time in culture and had become attenuated. Whatever the reason for the reduced pathogenicity of the Xen-39 strain, in retrospect, we should have first tested the strain in a small set of mice before performing the large lethality study with 50 animals, and we will not repeat this mistake.

Aerosolization of *Kp* ATCC 43816 resulted in 100% mortality in the BL/6 mice within 24 hours at the highest dose of 4.33 X 10^6 CFU, and within 6 days at the lowest dose of 6.06 X 10^3 CFU (Figure 5B). A literature review of other murine pneumonia models revealed that animals reaching internal temperatures below 32-34°C fail to recover, and instead rapidly deteriorate to

death within 24 to 48 hours (57-59). Because of this, we chose to euthanize all animals that reached an internal temperature below 34°C for two consecutive daily measurements. Interestingly, this seemed to be the only defining criteria for terminal illness, as none of the animals developed any other symptoms severe enough to warrant euthanasia (such as significant weight loss or physical symptoms). A subsequent literature review suggested that our finding may not be unusual, as other murine pneumonia models also reported no significant weight loss in terminally ill animals – only hypothermia and subdued behavior (57). However, employing this criterion alone for disease severity sacrifices sensitivity. Although the microchips are highly accurate, they can fall out or malfunction. Four of the twenty mice were removed from the study prior to reaching 34°C due to either chip malfunction or chip loss.

A major limitation of our pneumonia model is that it is based only on observable, physical symptoms of live animals. In order to create a more accurate model of *Kp* induced pneumonia, we would need to serially sacrifice animals throughout the experiment and remove the lungs for assays such as histopathological examination, quantification of viable bacteria, and lipid peroxidation (to estimate extent of tissue damage). However, given that our end goal is not to characterize the bacterial pneumonia itself-- but to assess how drug efficacy changes with different drug carriers-- we believe our temperature-based model is sufficient.

Ultimately, we determined that aerosolization of *Kp* ATCC 43816 results in 100% mortality within six days post-infection with doses as low as 10^3 CFU. We also determined that temperature monitoring is the best indicator of disease progression, as few mice developed any other typical symptoms of illness. These results will help us plan future antibiotic treatment studies and allow us to use disease progression and recovery as measurable outcomes of *Klebsiella* infection and surfactant-based antibiotic treatment.

We next focused on developing our image-based, pulmonary drug dispersion model. Using fluorescent dye as a tracer and drug surrogate, we developed a ready-to-use, *in vivo* model to characterize dispersion based on the ratio of fluorescence in peripheral lung regions to the fluorescence in the total lung region, denoted the P/T ratio (Figure 2). We then applied this model to show that our candidate surfactant carrier, FS-3100, increases pulmonary dispersion over water carriers when instilled into murine lungs.

Through the model development process, we learned that aerosolization of fluorophores with the technologies available to us will not result in measurable fluorescent signal, and instead adopted the IMIT instillation technique of delivery. We believe that aerosol delivery failed because the system we used delivers the dye solution at a rate greater than six liters per minute, which may dilute the fluorophores above detection capacity.

Though our initial goal was to deliver the fluorescent dye via aerosol, we are confident in our choice to use the IMIT instillation for our lung dispersion assays. Initial dispersion studies performed by our colleagues at Carnegie Mellon University assessed aerosolized FS-3100 spreading deposited onto *in vitro* surfaces; our model represents a 'more complex' system that bridges the gap between those *in vitro* studies and the human airways. Several animal studies have shown that instilled liquid surfactant carriers can improve pulmonary drug distribution (34, 60) and increase animal survival when administered with an antibiotic (38, 61); however, most of these studies test natural, exogenous pulmonary surfactant and related synthetic surfactants approved for use in SRT (34,38, 60,61). To our knowledge, we are the first to explore the possible clinical uses of the industrial fluorosurfactant, FS-3100. Additionally, our method uses novel *in vivo* imaging techniques to visualize lung dispersion using fluorescent particles, where as all other pulmonary dispersion assays we found either require lung removal or use radiolabeled particles as drug

surrogates (22,60,62-64). Our model is therefore superior to these other methods because 1) it does not require surgery or subject euthanasia; 2) it does not require special waste disposal; and 3) the fluorophores used are non-toxic and more stable than radiolabeled particles.

One limitation to this model is the use of murine lungs to model dispersion. Lung structure is a major factor contributing to inhaled particle deposition, and murine lungs differ significantly from human lungs; where human lungs have relatively symmetric, dichotomous branching patterns and two left lung lobes, murine lungs are strongly monopodial and only have one left lung lobe (65). Additionally, the small size of murine lungs makes instillation difficult and limits the physical range of possible droplet spreading. Now that we have successfully shown that FS-3100 increases pulmonary spreading in mice, however, we have grounds to use larger animals in future studies.

Another limitation to our model is the use of healthy, non-obstructed lungs to model dispersion. Though several murine models of cystic fibrosis exist, they are not without significant flaws and are beyond the scope of this study. Future experiments will need to take into consideration how the surfactant will perform in obstructed airways; however, here we have used healthy lungs to develop an initial model. Our study demonstrates that a surfactant carrier can significantly increase pulmonary drug dispersion of a drug surrogate when instilled into murine lungs and that this model is potentially useful for evaluating surfactants to improve pulmonary drug delivery.

5.1 PUBLIC HEALTH SIGNIFICANCE

The continued development of novel treatments for cystic fibrosis has increased the median life-expectancy for those living with CF to around 40-years of age, but some 80% of patients still die

from complications arising from persistent lung infections. Inhaled antibiotics are frequently prescribed for the treatment of such infections, yet their efficacy is limited by their ability to adequately reach infection sites in obstructed airways, and to do so in high enough concentrations to fully eradicate the microbes. In such cases, the chronic delivery of sub-par antibiotic doses to some parts of the lungs may actually act to increase selection of antibiotic resistant strains in those areas. The emergence of multi-resistant pathogens in CF patients is well documented, and several studies have shown that infection with such strains significantly worsens patient outcomes (66-69). Additionally, while inhaled antibiotics have proved more effective than traditional methods of delivery in suppressing infection, to date, none have been able to fully eradicate CF pathogens, nor have any been found to be consistently effective. Thus, it is imperative that we continue to develop better antibiotics for treating CF-associated lung infections.

Our study demonstrates that a surfactant carrier can significantly increase pulmonary dispersion of a drug surrogate when instilled into murine lungs. More research is needed to determine if this ability will hold when the surfactant is inhaled, or if it will translate to increased drug efficacy in obstructed human airways. We hope that future research can build upon our early results to create an optimal inhaled antibiotic capable of fully eradicating CF-related pulmonary infections and improving patient outcomes.

APPENDIX: MOUSE OBSERVATION SCORING SYSTEM

Weight loss: 0-4.9% = 1; 5-9.9% = 2; 10-14.9% = 3; 15.1-20% = 4; > 20% = euthanize promptly

Temperature: 34-39.9degC = 1; 40.0-40.9degC = 2; 41.0-41.9degC = 3; >41.9 = 4; <34 = euthanize promptly

Natural Behavior: Normal = 1; less peer interaction = 2; little peer interaction, less mobile = 3; no peer interaction, vocalization, restless or still = 4

Provoked Behavior: Normal = 1; subdued but normal when stimulated = 2; subdued even when stimulated = 3; unresponsive even when stimulated = 4

Appearance: Normal = 1; reduced grooming = 2; dull/rough coat or ocular/mucosal discharge = 3; hunched, piloerection, or respiratory distress = 4

Total Score:

5-9: Normal

10-15: Clinical illness; increase observations to every six hours

Any category > 3; Clinical illness; increase observations to every six hours

16 +: Moribund, euthanize promptly

BIBLIOGRAPHY

1. **Vankeerberghen A, Cuppens H, Cassiman J-J.** 2002. The cystic fibrosis transmembrane conductance regulator: an intriguing protein with pleiotropic functions. Journal of Cystic Fibrosis **1:**13-29.

2. **Castellani C, Cuppens H, Macek M, Jr., Cassiman JJ, Kerem E, Durie P, Tullis E, Assael BM, Bombieri C, Brown A, Casals T, Claustres M, Cutting GR, Dequeker E, Dodge J, Doull I, Farrell P, Ferec C, Girodon E, Johannesson M, Kerem B, Knowles M, Munck A, Pignatti PF, Radojkovic D, Rizzotti P, Schwarz M, Stuhrmann M, Tzetis M, Zielenski J, Elborn JS.** 2008. Consensus on the use and interpretation of cystic fibrosis mutation analysis in clinical practice. J Cyst Fibros **7:**179-196.

3. **Mornon JP, Lehn P, Callebaut I.** 2008. Atomic model of human cystic fibrosis transmembrane conductance regulator: membrane-spanning domains and coupling interfaces. Cell Mol Life Sci **65:**2594-2612.

4. **Quinton PM.** 1990. Cystic fibrosis: a disease in electrolyte transport. The FASEB Journal **4:**2709-2717.

5. **Verkman A, Song Y, Thiagarajah JR.** 2003. Role of airway surface liquid and submucosal glands in cystic fibrosis lung disease. American Journal of Physiology-Cell Physiology **284:**C2-C15.

6. **Hamosh A, FitzSimmons SC, Macek M, Knowles MR, Rosenstein BJ, Cutting GR.** 1998. Comparison of the clinical manifestations of cystic fibrosis in black and white patients. The Journal of pediatrics **132:**255-259.

7. **Morgan WJ, Butler SM, Johnson CA, Colin AA, FitzSimmons SC, Geller DE, Konstan MW, Light MJ, Rabin HR, Regelmann WE.** 1999. Epidemiologic study of cystic fibrosis: design and implementation of a prospective, multicenter, observational study of patients with cystic fibrosis in the US and Canada. Pediatric pulmonology **28:**231-241.

8. **Rosenstein BJ, Cutting GR.** 1998. The diagnosis of cystic fibrosis: a consensus statement. The Journal of pediatrics **132:**589-595.

9. **Moran A, Dunitz J, Nathan B, Saeed A, Holme B, Thomas W.** 2009. Cystic fibrosis–related diabetes: current trends in prevalence, incidence, and mortality. Diabetes care **32:**1626-1631.

10. **Paccou J, Zeboulon N, Combescure C, Gossec L, Cortet B.** 2010. The prevalence of osteoporosis, osteopenia, and fractures among adults with cystic fibrosis: a systematic literature review with meta-analysis. Calcif Tissue Int **86:**1-7.

11. **Feranchak AP, Sokol RJ.** Cholangiocyte biology and cystic fibrosis liver disease, p 471-488. *In* (ed), Copyright© 2001 by Thieme Medical Publishers, Inc., 333 Seventh Avenue, New York, NY 10001, USA. Tel.:+ 1 (212) 584-4662,

12. **Sawicki GS, Sellers DE, Robinson WM.** 2009. High treatment burden in adults with cystic fibrosis: challenges to disease self-management. J Cyst Fibros **8:**91-96.

13. **van Gool K, Norman R, Delatycki MB, Hall J, Massie J.** 2013. Understanding the costs of care for cystic fibrosis: an analysis by age and health state. Value Health **16:**345-355.

14. **Lyczak JB, Cannon CL, Pier GB.** 2002. Lung infections associated with cystic fibrosis. Clinical microbiology reviews **15:**194-222.

15. **Hart CA, Winstanley C.** 2002. Persistent and aggressive bacteria in the lungs of cystic fibrosis children. British medical bulletin **61:**81-96.

16. **Podschun R, Ullmann U.** 1998. Klebsiella spp. as nosocomial pathogens: epidemiology, taxonomy, typing methods, and pathogenicity factors. Clinical microbiology reviews **11:**589-603.

17. **Simona B, Brooks S, Sibte B, Sandeep K, Gupta J, Landman D, John Q.** 2007. Detection and Spread of Escherichia coli Possessing the Plasmid-Borne Carbapenemase KPC-2 in Brooklyn, New York. Clinical Infectious Diseases **44:**972-975.

18. **Leao RS, Pereira RH, Folescu TW, Albano RM, Santos EA, Junior LG, Marques EA.** 2011. KPC-2 carbapenemase-producing Klebsiella pneumoniae isolates from patients with Cystic Fibrosis. J Cyst Fibros **10:**140-142.

19. **Villegas MV, Lolans K, Correa A, Kattan JN, Lopez JA, Quinn JP, Colombian Nosocomial Resistance Study G.** 2007. First identification of Pseudomonas aeruginosa isolates producing a KPC-type carbapenem-hydrolyzing beta-lactamase. Antimicrob Agents Chemother **51:**1553-1555.

20. **Delfino E, Giacobbe DR, Del Bono V, Coppo E, Marchese A, Manno G, Morelli P, Minicucci L, Viscoli C.** 2015. First report of chronic pulmonary infection by KPC-3-producing and colistin-resistant Klebsiella pneumoniae sequence type 258 (ST258) in an adult patient with cystic fibrosis. Journal of clinical microbiology **53:**1442-1444.

21. **Geller DE.** 2009. Aerosol antibiotics in cystic fibrosis. Respiratory care **54:**658-670.

22. **Brown JS, Zeman KL, Bennett WD.** 2001. Regional deposition of coarse particles and ventilation distribution in healthy subjects and patients with cystic fibrosis. Journal of aerosol medicine **14:**443-454.

23. **Marcinkowski AL, Garoff S, Tilton RD, Pilewski JM, Corcoran TE.** 2008. Postdeposition dispersion of aerosol medications using surfactant carriers. Journal of aerosol medicine and pulmonary drug delivery **21:**361-370.

24. **De Backer W, Devolder A, Poli G, Acerbi D, Monno R, Herpich C, Sommerer K, Meyer T, Mariotti F.** 2010. Lung deposition of BDP/formoterol HFA pMDI in healthy volunteers, asthmatic, and COPD patients. Journal of aerosol medicine and pulmonary drug delivery **23:**137-148.

25. **Palmer LB.** 2000. Aerosolized antibiotics: current and future. Respiratory Care **45:**667.

26. **Lenney W, Edenborough F, Kho P, Kovarik JM.** 2011. Lung deposition of inhaled tobramycin with eFlow rapid/LC Plus jet nebuliser in healthy and cystic fibrosis subjects. J Cyst Fibros **10:**9-14.

27. **Ryan G, Singh M, Dwan K.** 2011. Inhaled antibiotics for long-term therapy in cystic fibrosis. The Cochrane Library.

28. **Drug label for BETHKIS–Tobramycin Inhalation Solution**. Food and Drug Administration. 2015. https://www.accessdata.fda.gov/drugsatfda_docs/label/2015/050753s018lbl.pdf

29. **Drug label for CAYSTON–Aztreonam for Inhalation Solution**. Food and Drug Administration. 2010. https://www.accessdata.fda.gov/drugsatfda_docs/label/2010/050814lbl.pdf

30. **Im Hof V, Gehr P, Gerber V, Lee M, Schürch S.** 1997. In vivo determination of surface tension in the horse trachea and in vitro model studies. Respiration physiology **109:**81-93.

31. **Kirkness JP, Christenson HK, Garlick SR, Parikh R, Kairaitis K, Wheatley JR, Amis TC.** 2003. Decreased surface tension of upper airway mucosal lining liquid increases upper airway patency in anaesthetised rabbits. J Physiol **547:**603-611.

32. **Khanal A, Sharma R, Corcoran TE, Garoff S, Przybycien TM, Tilton RD.** 2015. Surfactant Driven Post-Deposition Spreading of Aerosols on Complex Aqueous Subphases. 1: High Deposition Flux Representative of Aerosol Delivery to Large Airways. J Aerosol Med Pulm Drug Deliv **28:**382-393.

33. **Veldhuizen R, Nag K, Orgeig S, Possmayer F.** 1998. The role of lipids in pulmonary surfactant. Biochimica et Biophysica Acta (BBA)-Molecular Basis of Disease **1408:**90-108.

34. **Nimmo AJ, Carstairs JR, Patole SK, Whitehall J, Davidson K, Vink R.** 2002. Intratracheal Administration Of Glucocorticoids Using Surfactant As A Vehicle. Clinical & Experimental Pharmacology & Physiology **29:**661-665.

35. **Grotberg JB.** 2001. Respiratory fluid mechanics and transport processes. Annual Review of Biomedical Engineering **3:**421.

36. **Halpern D, Jensen O, Grotberg J.** 1998. A theoretical study of surfactant and liquid delivery into the lung. Journal of Applied Physiology **85:**333-352.

37. **Nikolov AD, Wasan DT, Chengara A, Koczo K, Policello GA, Kolossvary I.** 2002. Superspreading driven by Marangoni flow. Advances in colloid and interface science **96:**325-338.

38. **Veen Avt, Mouton JW, Gommers D, Lachmann B.** 1996. Pulmonary surfactant as vehicle for intratracheally instilled tobramycin in mice infected with Klebsiella pneumoniae. British journal of pharmacology **119:**1145-1148.

39. **Fajardo C, Levin D, Garcia M, Abrams D, Adamson I.** 1998. Surfactant versus saline as a vehicle for corticosteroid delivery to the lungs of ventilated rabbits. Pediatric research **43:**542-547.

40. **Kumar GP, Rajeshwarrao P.** 2011. Nonionic surfactant vesicular systems for effective drug delivery—an overview. Acta Pharmaceutica Sinica B **1:**208-219.

41. **Uchegbu IF, Vyas SP.** 1998. Non-ionic surfactant based vesicles (niosomes) in drug delivery. International Journal of Pharmaceutics **172:**33-70.

42. Kissa, E. 1994. Structure of fluorinated surfactants, p 2. *In* Kissa, E, Fluorinated surfactants: synthesis, properties, applications, Marcel Decker, New York, NY.

43. **Kovalchuk NM, Trybala A, Starov V, Matar O, Ivanova N.** 2014. Fluoro- vs hydrocarbon surfactants: why do they differ in wetting performance? Adv Colloid Interface Sci **210:**65-71.

44. **Caliper Life Sciences.** 2012. Living Image® 4.3.1 User's Manual – IVIS® SpectrumCT. Caliper Life Sciences, Waltham, MA.

45. **Koch K, Dew B, Corcoran TE, Przybycien TM, Tilton RD, Garoff S.** 2011. Surface tension gradient driven spreading on aqueous mucin solutions: a possible route to enhanced pulmonary drug delivery. Mol Pharm **8:**387-394.

46. **Harvey PR, Tarran R, Garoff S, Myerburg MM.** 2011. Measurement of the airway surface liquid volume with simple light refraction microscopy. American journal of respiratory cell and molecular biology **45:**592-599.

47. **Corcoran TE, Thomas KM, Garoff S, Tilton RD, Przybycien TM, Pilewski JM.** 2012. Imaging the postdeposition dispersion of an inhaled surfactant aerosol. J Aerosol Med Pulm Drug Deliv **25:**290-296.

48. **Stetten AZ, Moraca G, Corcoran TE, Tristram-Nagle S, Garoff S, Przybycien TM, Tilton RD.** 2016. Enabling Marangoni flow at air-liquid interfaces through deposition of aerosolized lipid dispersions. Journal of Colloid and Interface Science **484:**270-278.

49. **Sharma R, Khanal A, Corcoran TE, Garoff S, Przybycien TM, Tilton RD.** 2015. Surfactant Driven Post-Deposition Spreading of Aerosols on Complex Aqueous Subphases. 2: Low Deposition Flux Representative of Aerosol Delivery to Small Airways. J Aerosol Med Pulm Drug Deliv **28:**394-405.

50. **Sharma R, Corcoran TE, Garoff S, Przybycien TM, Swanson ER, Tilton RD.** 2013. Quasi-immiscible spreading of aqueous surfactant solutions on entangled aqueous polymer solution subphases. ACS Appl Mater Interfaces **5:**5542-5549.

51. **Lawrenz MB, Fodah RA, Gutierrez MG, Warawa J.** 2014. Intubation-mediated intratracheal (IMIT) instillation: a noninvasive, lung-specific delivery system. JoVE (Journal of Visualized Experiments)**:**e52261-e52261.

52. **Tan S, Gan C, Li R, Ye Y, Zhang S, Wu X, Yang YY, Fan W, Wu M.** 2015. A novel chemosynthetic peptide with beta-sheet motif efficiently kills Klebsiella pneumoniae in a mouse model. Int J Nanomedicine **10:**1045-1059.

53. **Berendt R.** 1978. Relationship of method of administration to respiratory virulence of Klebsiella pneumoniae for mice and squirrel monkeys. Infection and immunity **20:**581.

54. **Nishi T, Tsuchiya K.** 1980. Experimental respiratory tract infection with Klebsiella pneumoniae DT-S in mice: chemotherapy with kanamycin. Antimicrobial agents and chemotherapy **17:**494-505.

55. **Stephenson EH, Moeller RB, York CG, Young HW.** 1988. Nose-Only Versus Whole-Body Aerosol Exposure for Induction of Upper Respiratory Infections of Laboratory Mice. American Industrial Hygiene Association Journal **49:**128-135.

56. **Kort W, Hekking-Weijma J, TenKate M, Sorm V, VanStrik R.** 1998. A microchip implant system as a method to determine body temperature of terminally ill rats and mice. Laboratory animals **32:**260-269.

57. **Bolister N, Johnson H, Wathes C.** 1992. The ability of airborne Klebsiella pneumoniae to colonize mouse lungs. Epidemiology and infection **109:**121.

58. **Soothill J, Morton D, Ahmad A.** 1992. The HID50 (hypothermia-inducing dose 50): an alternative to the LD50 for measurement of bacterial virulence. International journal of experimental pathology **73:**95.

59. **Wong JP, Saravolac EG, Clement JG, Nagata LP.** 1997. Development of a murine hypothermia model for study of respiratory tract influenza virus infection. Laboratory animal science **47:**143-147.

60. **Kharasch VS, Sweeney TD, Fredberg J, Lehr J, Damokosh AI, Avery ME, Brain JD.** 1991. Pulmonary surfactant as a vehicle for intratracheal delivery of technetium sulfur colloid and pentamidine in hamster lungs. American Review of Respiratory Disease **144:**909-913.

61. **Hughes WT, Sillos EM, LaFon S, Rogers M, Woolley JL, Davis C, Studenberg S, Pattishall E, Freeze T, Snyder G, Staton S.** 1998. Effects of Aerosolized Synthetic Surfactant, Atovaquone, and the Combination of These on Murine Pneumocystis carinii Pneumonia. The Journal of Infectious Diseases **177:**1046-1056.

62. **Yi D, Price A, Panoskaltsis-Mortari A, Naqwi A, Wiedmann TS.** 2010. Measurement of the distribution of aerosols among mouse lobes by fluorescent imaging. Anal Biochem **403:**88-93.

63. **Yi D, Wiedmann TS, Naqwi A, Price AP, Panoskaltsis-Mortari A.** 2012. Distribution of aerosols in murine obliterative bronchiolitis lungs by fluorescent imaging. Experimental lung research **38:**325-332.

64. **Cheng Y, Irshad H, Kuehl P, Holmes T, Sherwood R, Hobbs C.** 2008. Lung deposition of droplet aerosols in monkeys. Inhalation toxicology **20:**1029-1036.

65. **Irvin CG, Bates JH.** 2003. Measuring the lung function in the mouse: the challenge of size. Respiratory Research **4:**1.

66. **Lechtzin N, John M, Irizarry R, Merlo C, Diette GB, Boyle MP.** 2006. Outcomes of adults with cystic fibrosis infected with antibiotic-resistant Pseudomonas aeruginosa. Respiration **73:**27-33.

67. **Oliver A, Cantón R, Campo P, Baquero F, Blázquez J.** 2000. High frequency of hypermutable Pseudomonas aeruginosa in cystic fibrosis lung infection. Science **288:**1251-1253.

68. **Davies G, McShane D, Davies J, Bush A.** 2003. Multiresistant Pseudomonas aeruginosa in a pediatric cystic fibrosis center: natural history and implications for segregation. Pediatric pulmonology **35:**253-256.

69. **Molina A, Del Campo R, Maiz L, Morosini MI, Lamas A, Baquero F, Canton R.** 2008. High prevalence in cystic fibrosis patients of multiresistant hospital-acquired methicillin-resistant Staphylococcus aureus ST228-SCCmecI capable of biofilm formation. J Antimicrob Chemother **62:**961-967.